This article has been accepted for publication in a future issue of this journal, but has not been fully edited. Content may change prior to final publication. Citation information: DOI 10.1109/TSP.2017.2711534, IEEE Transactions on Signal Processing

Parallel Equalization Structure for MIMO FBMC-OQAM Systems under Strong Time and Frequency Selectivity

François Rottenberg, *Student Member, IEEE,* Xavier Mestre, *Senior Member, IEEE,* Dmitry Petrov, *Member, IEEE,* François Horlin, *Member, IEEE,* and Jérôme Louveaux, *Member, IEEE*

***Abstract*—Offset-QAM-based filterbank multicarrier (FBMC-OQAM) has been shown to be a promising alternative to cyclic prefix-orthogonal frequency division multiplexing (CP-OFDM) for the future generation of wireless communication systems. Unfortunately, as the channel gets more selective in time and frequency, the FBMC-OQAM orthogonality is progressively destroyed and distortion appears after the demodulation process at the receiver. While channel frequency selectivity has been very widely studied in the FBMC literature, the impact of time selectivity of the channel has not received that much attention. In this paper, the effect of the two types of selectivity on a multiple-input multiple-output (MIMO) FBMC system is characterized and a parallel equalization structure that can compensate for the doubly dispersive nature of the channel is proposed. This design uses multiple analysis filterbanks (AFB) and extends previous approaches that were dealing only with channel frequency selectivity. A theoretical approximation of the remaining distortion after equalization is given. The study is performed for a general MIMO system but can also be particularized to single-input single-output (SISO) systems. Simulation results demonstrate the high efficiency of the proposed receiver structure and the accuracy of the theoretical approximations is verified.**

***Index Terms*—FBMC-OQAM, doubly selective channels, parallel equalization.**

I. Introduction

Offset-QAM-based filterbank multicarrier (FBMC-OQAM) has been shown to be an attractive alternative to cyclic prefix-orthogonal frequency division multiplexing (CP-OFDM) as the new modulation format in the next generations of wireless communication systems. It is well known that the FFT filters inherent to CP-OFDM generate high spectral leakage. As opposed to CP-OFDM, FBMC-OQAM uses a pulse shape which is more spread out in time. This results in a much better time-frequency localization of the prototype pulse [1], making the system more robust to timing and carrier frequency offsets [2]. Further, it gives more flexibility for the spectrum utilization. For instance, compared to a CP-OFDM system, it greatly decreases the number of guard band subcarriers on the edges of the system bandwidth left inactive to respect spectral emission masks [3] or between unsynchronized users [4]. Moreover, FBMC-OQAM does not require the use of a cyclic prefix (CP), which again increases the spectral efficiency of the system [3].

The advantages of FBMC-OQAM come at the expense of an increase in the system implementation complexity. More specifically, this modulation generates a particular interference pattern, which can easily be taken care of if the channel is mildly frequency selective and slowly changing over time but requires additional signal processing in more complex propagation environments [5], [6]. Furthermore, one should note that to achieve higher spectral selectivity, the prototype pulse needs to be more spread out in the time domain, which induces more latency and might be detrimental for short burst transmissions. Pre-loading techniques and tail shortening algorithms were designed to limit this effect [3], [7]–[9].

If the channel is slowly varying in time and frequency, single-tap equalization is sufficient to compensate for the channel distortion and restore the FBMC-OQAM orthogonality. However, as the channel gets more selective in time and frequency, distortion will appear and FBMC will suffer from so-called intrinsic interference caused by inter-symbol interference (ISI) and inter-carrier interference (ICI). In the literature, many papers have proposed algorithms to compensate for the frequency selectivity of the channel. Various authors have studied the problem in the single-antenna case [5], [10]–[12] and later on for the MIMO case [6], [13], [14]. Most of these approaches are based on the design of multi-tap fractionally spaced equalizers. One should note that multi-tap equalizers have a larger complexity and add an additional delay to the demodulation process. In a multi-user MIMO context, [15] proposes to keep a single-tap design and to use the extra base station antennas as extra degrees of freedom to cancel the distortion induced by the channel frequency selectivity.

On the contrary, the case of time selective channels, i.e., the fact that the channel rapidly changes over time, has not been extensively studied in the FBMC literature. This issue is of crucial importance for the future of wireless communications. Two examples of application are high speed trains and satellite communications. In [16]–[18], different

The research reported herein was partly funded by Fonds pour la Formation à la Recherche dans l'Industrie et dans l'Agriculture, by the Catalan and Spanish governments under grants 2014SGR1567 and TEC2014-59255-C3-1 and by the Ministry of Education and Science of the Russian Federation (the Agreement number 02.a03.21.0008).

François Rottenberg and Jérôme Louveaux are with the Université catholique de Louvain, 1348 Louvain-la-Neuve, Belgium (e-mail: francois.rottenberg@uclouvain.be;jerome.louveaux@uclouvain.be).

Xavier Mestre is with the Centre Tecnolgic de Telecomunicacions de Catalunya, 08860 Barcelona, Spain (e-mail: xavier.mestre@cttc.cat).

Dmitry Petrov is with Magister Solutions Ltd, 40720 Jyväskylä, Finland (e-mail:dmitry.petrov@magister.fi) and with Peoples' Friendship University of Russia, Moscow, Russian Federation.

François Rottenberg and François Horlin are with the Université libre de Bruxelles, 1050 Brussel, Belgium (e-mail: fhorlin@ulb.ac.be).

This article has been accepted for publication in a future issue of this journal, but has not been fully edited. Content may change prior to final publication. Citation information: DOI 10.1109/TSP.2017.2711534, IEEE Transactions on Signal Processing

multicarrier modulations schemes proposed for 5G systems, including CP-OFDM and FBMC-OQAM modulations, are compared under high speed scenarios. Their main result is that FBMC-OQAM provides more robustness to channel dispersion with respect to conventional CP-OFDM. In [19], [20], the authors propose adaptive equalizers for doubly selective channels in MIMO FBMC-OQAM systems. The work of [21] addresses the same problem by designing a fractionally spaced per-subcarrier equalizer, taking into account the interference coming from neighboring subcarriers and adjacent symbols in time. In [22], the mean squared error (MSE) of the received symbols for doubly dispersive channel is analyzed for SISO FBMC systems with classical single-tap equalization. From the channel estimation point of view, the authors in [23] propose a general framework for compressive estimation of doubly selective channels in multicarrier systems. Other works study the effect of varying the prototype pulse shape to deal with doubly selective channels [24], [25].

In this paper, we first characterize the effect of time and frequency variations of the channel on the FBMC transceiver chain. Second, we propose a new receiver structure for MIMO FBMC-OQAM systems that can compensate for both the time and frequency selectivity of the channel. This receiver uses multiple analysis filterbanks (AFB) working in parallel on the received signal. Each AFB is using a different derivative of the prototype pulse with respect to time and frequency. The demodulated symbols coming from each parallel AFB are then equalized and re-combined in order to mitigate the distortion caused by the channel variations. This processing does not require any additional delay as opposed to multi-tap equalizers and has a relatively low complexity of implementation. Furthermore, an analytical approximation of the residual distortion and noise power after equalization is given, which results in a very compact expression, as compared with [22]. The proposed parallel equalization structure may be seen as an extension of the work of [26], [27] to the doubly selective channel case. Another related work that aimed at characterizing the FBMC distortion based on the same approach but restricted to the frequency selective only case, was performed in [28]–[30].

The rest of this paper is structured as follows. Section II details the system model for a general FBMC-OQAM MIMO transceiver and proposes different orders of approximation of the demodulated symbol for doubly selective channels. Section III proposes the new parallel receiver structure and gives a theoretical expression of the residual distortion and noise power. Section IV validates the accuracy of the distortion approximation and the performance of the proposed equalization structure. Finally, Section V concludes the paper.

A. Notations

Vectors and matrices are denoted by bold lowercase and uppercase letters, respectively (resp.). Superscripts *, ^{T} and ^{H} stand for conjugate, transpose and Hermitian transpose operators. The symbols tr, $\mathbb{E}$, $\Im$ and $\Re$ denote the trace, expectation, imaginary and real parts, respectively. $\jmath$ is the imaginary unit. The operator $\|\mathbf{A}\|$ returns the square root of the maximum eigenvalue of the matrix $\mathbf{A}^H\mathbf{A}$. $O(x)$ denotes a quantity that decays to zero at least as the same rate as x. $\mathbf{I}_N$ denotes the identity matrix of order N. $\otimes$ stands for the Kronecker product and $\delta[n]$ is the Kronecker delta.

TABLE I
NOTATIONS OF THE FBMC-OQAM COMMUNICATION LINK UNDER CONSIDERATION.

$2M$	Number of subcarriers
$2N_s$	Number of real-valued multicarrier symbols
T	Multicarrier symbol period
$T/2M$	Sampling period
N_T, N_R	Number of transmit, receive antennas
κ	Overlapping factor

II. System Model

A. FBMC-OQAM transmission model

Let us consider an FBMC-OQAM communication link, as depicted in Fig. 1, the parameters of which are summarized in Table I. The transmitter and receiver are equipped with N_T and N_R antennas respectively. We assume pure spatial multiplexing, so that the number of streams is equal to N_T, with $N_R \geq N_T$. The number of subcarriers is denoted by $2M$. The real-valued symbols, denoted by $\mathbf{d}_{m,l} \in \mathbb{R}^{N_T \times 1}$, correspond to the symbols transmitted at subcarrier m and multicarrier symbol l. The number of real-valued multicarrier symbols transmitted per antenna is denoted by $2N_s$. Furthermore, the symbols $\mathbf{d}_{m,l}$ are assumed bounded, independent and identically distributed random variables with zero mean and variance $P_s/2$.[1] These symbols are FBMC-OQAM modulated using a prototype pulse $p[n]$ of length $2M\kappa$, where κ is the overlapping factor. The transmitted signal $\mathbf{s}[n] \in \mathbb{C}^{N_T \times 1}$ can be written as

$$\mathbf{s}[n] = \sum_{l=0}^{2N_s-1} \sum_{m=0}^{2M-1} \mathbf{d}_{m,l} p_{m,l}[n],$$

where $p_{m,l}[n] = \jmath^{l+m} p[n - lM] e^{\jmath \frac{2\pi}{2M} m(n - \frac{2M\kappa-1}{2})}$ and where $\mathbf{s}[n]$ is non zero only for $n = 0, \ldots, 2\tilde{N}_s M - 1$. The quantity $\tilde{N}_s$, defined as $\tilde{N}_s = \frac{2N_s+2\kappa-1}{2}$, is introduced in order to simplify the expressions in the following. We denote by $\boldsymbol{\mathcal{H}}[b, n] \in \mathbb{C}^{N_R \times N_T}$ the time-variant channel impulse response at time instant n and corresponding to delay b. The received signal, denoted by $\mathbf{r}[n] \in \mathbb{C}^{N_R \times 1}$, is given by

$$\mathbf{r}[n] = \sum_{b=-\infty}^{+\infty} \boldsymbol{\mathcal{H}}[b, n] \mathbf{s}[n - b]. \tag{1}$$

Note that the additive noise effect has been omitted. Since the noise is not correlated with the data, its impact may be studied independently, as will be shown later. The received signal $\mathbf{r}[n]$ is FBMC-OQAM demodulated using prototype pulse $g[n]$ of length $2M\kappa$. The signal after demodulation, at subcarrier m_0

[1]The factor $1/2$ comes from the fact that P_s is the variance of the complex QAM symbol while $P_s/2$ is the variance of the related real PAM symbol.

This article has been accepted for publication in a future issue of this journal, but has not been fully edited. Content may change prior to final publication. Citation information: DOI 10.1109/TSP.2017.2711534, IEEE Transactions on Signal Processing

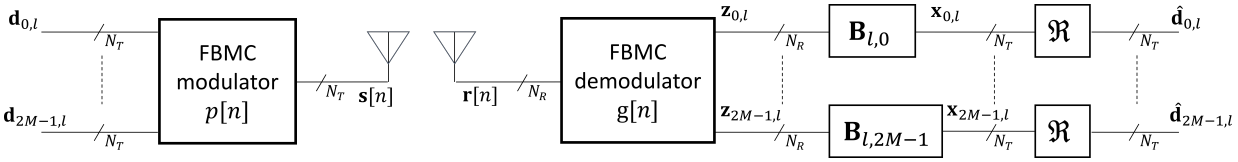

Fig. 1. Classical offset-QAM-based filterbank multicarrier transceiver chain (FBMC stands for filterbank multicarrier).

and multicarrier symbol l_0, denoted by $\mathbf{z}_{m_0,l_0} \in \mathbb{C}^{N_R \times 1}$, may be written as

$$\mathbf{z}_{m_0,l_0} = \sum_{n=0}^{2M\kappa-1} \mathbf{r}[n] g^*_{m_0,l_0}[n] \tag{2}$$
$$= \sum_{l=0}^{2N_s-1} \sum_{m=0}^{2M-1} \sum_{n=0}^{2M\kappa-1} \sum_{b=-\infty}^{+\infty} \boldsymbol{\mathcal{H}}[b,n] \mathbf{d}_{m,l} p_{m,l}[n-b] g^*_{m_0,l_0}[n],$$

where $g_{m,l}[n] = \jmath^{l+m} g[n-lM] e^{\jmath \frac{2\pi}{2M} m(n - \frac{2M\kappa-1}{2})}$. As it can be seen, the effect of the channel $\boldsymbol{\mathcal{H}}[b,n]$ on $\mathbf{z}_{m_0,l_0}$ is a mixed function of the transmitted data, channel and pulses. Approximations can be used to simplify the expression of $\mathbf{z}_{m_0,l_0}$. In the following, we first describe the classical approximation made in most of the FBMC literature and its limitations. Thereafter, we will propose our improved approximation of the demodulated symbol, which does not make any assumptions on the level of time and frequency selectivity of the channel.

Commonly, in most of the FBMC literature, the channel is assumed to remain constant over the transmit and receive pulse durations. Furthermore, the channel is typically assumed to be frequency flat at the subcarrier level. Under these conditions and if the pulses $p[n]$ and $g[n]$ are well localized in time and frequency, an approximation of $\mathbf{z}_{m_0,l_0}$ is given by

$$\mathbf{z}_{m_0,l_0} \approx \mathbf{H}_{m_0,l_0} \sum_{l=0}^{2N_s-1} \sum_{m=0}^{2M-1} \mathbf{d}_{m,l} \sum_{n=0}^{2M\kappa-1} p_{m,l}[n] g^*_{m_0,l_0}[n],$$

where $\mathbf{H}_{m_0,l_0} = \sum_{b=-\infty}^{+\infty} \boldsymbol{\mathcal{H}}[b, l_0 M + \frac{2M\kappa-1}{2}] e^{-\jmath \frac{2\pi}{2M} b m_0}$ is the time varying channel frequency response evaluated at the subcarrier and multicarrier symbol of interest. We will refer to this approximation as a 0-th order approximation of $\mathbf{z}_{m_0,l_0}$, that we denote by $\mathbf{z}^{(0,0)}_{m_0,l_0}$. To simplify notations, we define $\mathbf{y}_{m_0,l_0} \in \mathbb{C}^{N_T \times 1}$ as

$$\mathbf{y}_{m_0,l_0} = \sum_{l=0}^{2N_s-1} \sum_{m=0}^{2M-1} \mathbf{d}_{m,l} \sum_{n=0}^{2M\kappa-1} p_{m,l}[n] g^*_{m_0,l_0}[n]. \tag{3}$$

The samples $\mathbf{y}_{m_0,l_0}$ can be seen as the complex demodulated symbols at subcarrier m_0 and multicarrier symbol l_0, if the symbols $\mathbf{d}_{m,l}$ are FBMC-OQAM modulated using a prototype pulse $p[n]$, demodulated using a prototype pulse $g[n]$ and for an ideal channel, i.e., $\boldsymbol{\mathcal{H}}[b,n] = \delta[b]\mathbf{I}_{N_T}$. In other words, the samples $\mathbf{y}_{m_0,l_0}$ would be the output of a synthesis filterbank and an AFB placed back-to-back. Moreover, if the pulses $p[n]$ and $g[n]$ are perfect reconstruction pulses, one will have $\mathbf{d}_{m_0,l_0} = \Re(\mathbf{y}_{m_0,l_0})$. Note that $\mathbf{z}^{(0,0)}_{m_0,l_0}$ can be rewritten as

$$\mathbf{z}^{(0,0)}_{m_0,l_0} = \mathbf{H}_{m_0,l_0} \mathbf{y}_{m_0,l_0}.$$

The accuracy of the approximation $\mathbf{z}^{(0,0)}_{m_0,l_0}$ critically depends on the channel variations in the time and frequency domain. As the channel gets more time and/or frequency selective, the approximation will deteriorate. Classically, the receiver then applies a per-subcarrier decoding (equalizing) matrix $\mathbf{B}_{m_0,l_0} \in \mathbb{C}^{N_T \times N_R}$

$$\mathbf{x}_{m_0,l_0} = \mathbf{B}_{m_0,l_0} \mathbf{z}_{m_0,l_0} \approx \mathbf{B}_{m_0,l_0} \mathbf{H}_{m_0,l_0} \mathbf{y}_{m_0,l_0}$$

and the transmitted symbol $\mathbf{d}_{m_0,l_0}$ is estimated by taking the real part of $\mathbf{x}_{m_0,l_0}$, i.e., $\hat{\mathbf{d}}_{m_0,l_0} = \Re(\mathbf{x}_{m_0,l_0})$. If $\mathbf{B}_{m_0,l_0}\mathbf{H}_{m_0,l_0} = \mathbf{I}_{N_T}$, if the channel is not too selective and if the additive noise power is not too large, one can expect to get $\hat{\mathbf{d}}_{m_0,l_0}$ close to $\mathbf{d}_{m_0,l_0}$.

B. Channel model and prototype pulses

The work of [26] initially proposed the idea of considering higher order approximations of the demodulated signal $\mathbf{z}_{m_0,l_0}$ in the presence of channel frequency selectivity. In this paper, we extend the approach of [26] to doubly selective channels. To be able to write this higher order approximation of the demodulated symbol, we need to give a deeper description of the channel model. In the same way, smoothness conditions on the prototype pulses are necessary.

1) Channel model: Let us introduce the continuous time-frequency response of the channel, denoted by $\mathbf{H}(\omega, t)$ and defined in terms of normalized time and angular frequency, i.e., $t \in [0,1], \omega \in [0, 2\pi]$. The normalized time $t = 0$ denotes the beginning of the data transmission and $t = 1$, its end or unnormalized time $\tilde{N}_s T$ [s]. The normalized angular frequency $\omega = 0$ and $\omega = 2\pi$ corresponds to the edges of the system bandwidth, i.e., unnormalized frequencies 0 and $\frac{2M}{T}$ [Hz].

Since the function $\mathbf{H}(\omega, t)$ is limited to unnormalized frequency $\frac{2M}{T}$ and time $\tilde{N}_s T$, we know from the Shannon sampling theorem that the inverse Fourier transform of $\mathbf{H}(\omega, t)$ with respect to frequency ω can be sampled in the delay domain with a spacing $\frac{T}{2M}$, without causing any aliasing in the frequency domain. Similarly, the Fourier transform of $\mathbf{H}(\omega, t)$ with respect to time t can be sampled in the Doppler domain with a spacing $\frac{1}{\tilde{N}_s T}$. Hence, $\mathbf{H}(\omega, t)$ is equivalently defined by the discrete-delay-Doppler spreading function of the channel [31], which we denote by $\boldsymbol{\Psi}[b, \nu]$. The index b denotes the delay tap index while ν denotes the Doppler tap index. The

This article has been accepted for publication in a future issue of this journal, but has not been fully edited. Content may change prior to final publication. Citation information: DOI 10.1109/TSP.2017.2711534, IEEE Transactions on Signal Processing

functions $\mathbf{H}(\omega,t)$ and $\mathbf{\Psi}[b,\nu]$ are related through the relations

$$\begin{aligned}\mathbf{H}(\omega,t) &= \sum_{b=-\infty}^{+\infty}\sum_{\nu=-\infty}^{+\infty}\mathbf{\Psi}[b,\nu]e^{\jmath\left(\frac{\omega 2M}{T}\right)\left(\frac{bT}{2M}\right)}e^{-\jmath 2\pi\left(t\tilde{N}_sT\right)\left(\frac{\nu}{\tilde{N}_sT}\right)}\\ &= \sum_{b=-\infty}^{+\infty}\sum_{\nu=-\infty}^{+\infty}\mathbf{\Psi}[b,\nu]e^{-\jmath\omega b}e^{\jmath 2\pi t\nu}, \qquad (4)\\ \mathbf{\Psi}[b,\nu] &= \frac{1}{2\pi}\int_0^{2\pi}\left[\int_0^1\mathbf{H}(\omega,t)e^{-\jmath 2\pi t\nu}dt\right]e^{\jmath\omega b}\,d\omega.\end{aligned}$$

Functions $\mathbf{H}(\omega,t)$ and $\mathbf{\Psi}[b,\nu]$ equivalently define the channel and all channel frequency quantities can be derived from them. Equation (4) highlights the fact that $\mathbf{H}(\omega,t)$ can be seen as the linear superposition of multiple scatterers, each having a particular delay and Doppler shift. The time-variant channel impulse response $\boldsymbol{\mathcal{H}}[b,n]$ at time instant n and corresponding to delay b can be obtained from $\mathbf{\Psi}[b,\nu]$ as

$$\boldsymbol{\mathcal{H}}[b,n] = \sum_{\nu=-\infty}^{+\infty}\mathbf{\Psi}[b,\nu]e^{\jmath\frac{2\pi}{2\tilde{N}_sM}n\nu},$$

for $n=0,\ldots,2\tilde{N}_sM-1$.

The derivatives of the channel with respect to time and frequency at the subcarrier and multicarrier symbol of interest can also be expressed as a function of $\mathbf{\Psi}[b,\nu]$

$$\begin{aligned}\mathbf{H}_{m,l}^{(q,r)} &= \frac{d^q}{d\omega^q}\frac{d^r}{dt^r}\mathbf{H}(\omega,t)\Big|_{\omega=\omega_m,t=t_l} \qquad (5)\\ &= \sum_{b=-\infty}^{+\infty}\sum_{\nu=-\infty}^{\infty}(-\jmath b)^q(\jmath 2\pi\nu)^r\mathbf{\Psi}[b,\nu]e^{-\jmath\omega_m b+\jmath 2\pi t_l\nu},\end{aligned}$$

for $l=0,\ldots,2N_s-1$, $m=0,\ldots,2M-1$ and where we defined $\omega_m=\frac{2\pi}{2M}m$ and $t_l=\frac{1}{2\tilde{N}_sM}(lM+\frac{2M\kappa-1}{2})$. Note that $\mathbf{H}_{m,l}^{(0,0)}=\mathbf{H}_{m,l}$. Equation (5) highlights the fact that the variations of $\mathbf{H}(\omega,t)$ with respect to frequency and time can be related to the support of $\mathbf{\Psi}[b,\nu]$. If the function $\mathbf{\Psi}[b,\nu]$ is very spread out in the delay and/or Doppler domains, one can expect large variations of $\mathbf{H}(\omega,t)$ in the frequency and/or time domains respectively. To characterize those variations, we make the following assumption:

$(\mathbf{As1})$ The spreading function $\mathbf{\Psi}[b,\nu]$ is assumed to be causal and finitely supported in the delay and Doppler domains (as was assumed in [23]). This implies that $\mathbf{\Psi}[b,\nu]$ is non zero only for $b=0,\ldots,L_b$ and $\nu=-L_\nu,\ldots,L_\nu$. Moreover, we assume that the parameters L_b and L_ν are related to the maximal delay τ_{max} [s] and Doppler shift f_d [Hz] of the underlying analog channel, given by $L_b=\lfloor\frac{\tau_{max}2M}{T}\rfloor$ and $L_\nu=\lfloor f_d\tilde{N}_sT\rfloor$ with T being the multicarrier symbol period. The channel is assumed to be perfectly known by the receiver. Furthermore, we assume that

$$\begin{aligned}\inf_{(\omega,t)\in[0,2\pi]\times[0,1]}\lambda_{\min}\left(\mathbf{H}^H(\omega,t)\mathbf{H}(\omega,t)\right)>0,\\ \sup_{(\omega,t)\in[0,2\pi]\times[0,1]}\lambda_{\max}\left(\mathbf{H}^H(\omega,t)\mathbf{H}(\omega,t)\right)<+\infty\end{aligned}$$

where $\lambda_{\min}(\mathbf{A})$ and $\lambda_{\max}(\mathbf{A})$ denote the minimum and maximum eigenvalue of matrix $\mathbf{A}$ respectively.

Intuitively, $(\mathbf{As1})$ implies that the channel can be equivalently described by the combination of the effects of a finite number of scatterers, such that the number of delay taps and Doppler shifts are finite. Further, it implies that the channel is periodic in time and frequency, i.e., $\mathbf{H}(\omega,0)=\mathbf{H}(\omega,1)$ and $\mathbf{H}(0,t)=\mathbf{H}(2\pi,t)$, which makes sense if a sufficiently large observation window is used both in time and frequency. The equivalent channel should then be zero at the edges due to the time-frequency windowing effect of the analog filters at the transmitter and the receiver. Still, the channel model remains quite general under $(\mathbf{As1})$. For instance, it can address the special cases of a timing or carrier frequency offset. A timing offset of x samples would be modeled by imposing that $\mathbf{\Psi}[b,\nu]=\mathbf{0}$ if $b<x$.

Moreover, $(\mathbf{As1})$ implies that the channel is perfectly known at the receiver. In practice, this is of course not the case and the receiver should estimate the function $\mathbf{\Psi}[b,\nu]$ based on pilots scattered in time and frequency inside the transmitted frame. If the support of the function $\mathbf{\Psi}[b,\nu]$ is not known in advance, one has to estimate the channel frequency response and its derivatives at each subcarrier and multicarrier symbol of interest by interpolation between the scattered pilots. Due to the OQAM modulation and the MIMO scenario, the pilot symbols may be impacted by ISI, ICI and inter-antenna interference. Many works in the literature have looked at this issue, see [32] for a general review or [33], [34] for more recent works on the challenges and solutions in pilot-aided channel estimation for FBMC-OQAM systems.

2) Prototype pulse: We introduce the following assumptions on the prototype pulses.

$(\mathbf{As2})$ The transmit and receive prototype pulses $p[n]$ and $g[n]$ are of the perfect reconstruction type and of energy normalized to one. They are either symmetric or anti-symmetric. Furthermore, $g[n]$ is obtained by the discretization of an analog waveform $\tilde{g}(t):\mathbb{R}\to\mathbb{R}$ so that

$$g[n]=\tilde{g}\left(\left(n-\frac{2M\kappa-1}{2}\right)\frac{1}{2M}\right),$$

for $n=0,\ldots,2M\kappa-1$ and zero elsewhere. The additional shift of $\frac{2M\kappa-1}{2}$ units is performed in order to obtain a causal pulse. Further, $\tilde{g}(t)$ is analytic and only non zero if $t\in[-\kappa/2,\kappa/2]$.

Moreover, we define $g^{(q,r)}[n]$ as

$$g^{(q,r)}[n]=\tilde{g}^{(q,r)}\left(\left(n-\frac{2M\kappa-1}{2}\right)\frac{1}{2M}\right),$$

where $\tilde{g}^{(q,r)}(t)=\frac{d^q}{dt^q}(t^r\tilde{g}(t))$. Further, we define $\mathbf{y}_{m_0,l_0}^{(q,r)}$ as

$$\mathbf{y}_{m_0,l_0}^{(q,r)}=\sum_{l=0}^{2N_s-1}\sum_{m=0}^{2M-1}\mathbf{d}_{m,l}\sum_{n=0}^{2M\kappa-1}p_{m,l}[n]g_{m_0,l_0}^{(q,r)*}[n], \qquad (6)$$

where $g_{m_0,l_0}^{(q,r)}[n]=\jmath^{l_0+m_0}g^{(q,r)}[n-l_0M]e^{\jmath\frac{2\pi}{2M}m_0(n-\frac{2M\kappa-1}{2})}$. Note that $\mathbf{y}_{m_0,l_0}^{(0,0)}=\mathbf{y}_{m_0,l_0}$ as defined in (3) and that, for perfect reconstruction pulses $p[n]$ and $g[n]$, the perfect reconstruction property is not generally fulfilled by $p[n]$ and $g^{(q,r)}[n]$ if $(q,r)\neq(0,0)$.

This article has been accepted for publication in a future issue of this journal, but has not been fully edited. Content may change prior to final publication. Citation information: DOI 10.1109/TSP.2017.2711534, IEEE Transactions on Signal Processing

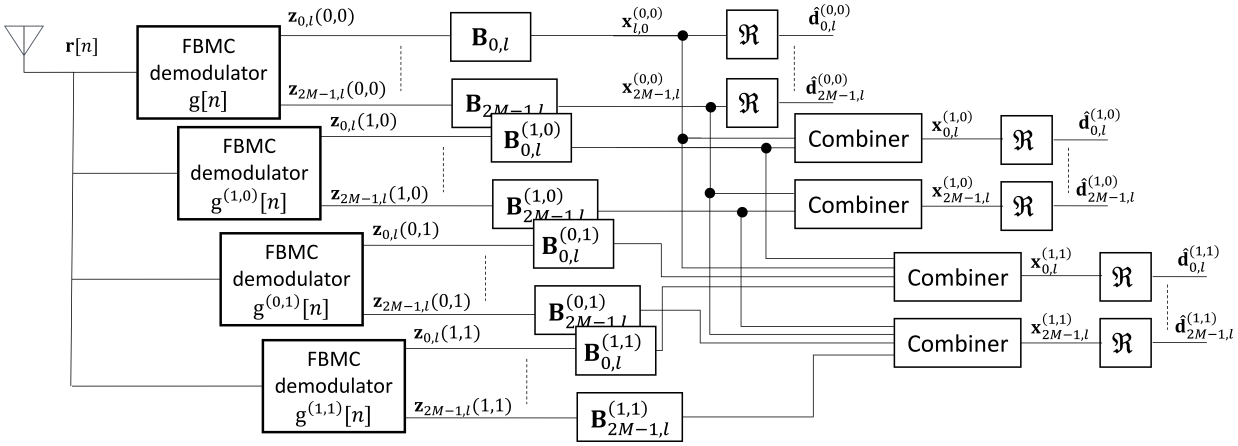

Fig. 2. Parallel equalization structure at the receiver for different designs: $Q=0, R=0$ (classical), $Q=1, R=0$ and $Q=1, R=1$.

C. Higher order approximation of the demodulated symbol

We are now in the position of introducing the main result of this section.

Proposition II.1. *Under* $(\mathbf{As1})-(\mathbf{As2})$*, an approximation of* $\mathbf{z}_{m_0,l_0}$ *of order* Q *with respect to channel variation in frequency and of order* R *with respect to channel variation in time is given by*

$$\mathbf{z}_{m_0,l_0}^{(Q,R)} = \sum_{r=0}^{R}\sum_{q=0}^{Q} \frac{\jmath^q}{(2M)^q q!(\tilde{N}_s)^r r!}\mathbf{H}_{m_0,l_0}^{(q,r)}\mathbf{y}_{m_0,l_0}^{(q,r)} \qquad (7)$$

and as $\frac{\tau_{max}}{T}\to 0$ *and* $f_dT\to 0$*, the approximation error can be bounded by*

$$\left\|\mathbf{z}_{m_0,l_0}-\mathbf{z}_{m_0,l_0}^{(Q,R)}\right\| = O\left(\left(\frac{\tau_{max}}{T}\right)^Q\right)+O\left((f_dT)^R\right). \qquad (8)$$

Proof. The proof is based on the truncation of a double Taylor expansion of the channel and the pulse with respect to time and frequency. See Appendix VI-A for the complete proof. □

Equation (7) gives more understanding of what is happening to the demodulated signal in the presence of channel selectivity. As the channel gets more selective, the derivatives of the channel $\mathbf{H}_{m_0,l_0}^{(q,r)}$ are amplified and distortion will be superimposed on the demodulated signal. Equation (8) shows that the approximation is more accurate when $\frac{\tau_{max}}{T}$ and Tf_d are small. As one would expect, a larger symbol period T is beneficial regarding frequency selectivity since the maximal delay of the channel will be smaller with respect to the symbol duration. At the same time, a larger T means that the channel will have stronger variations in time during one symbol period, which is detrimental regarding time selectivity. In practice, the choice of T should be made according to a trade-off between time and frequency selectivity. For a fixed T, the approximation is more accurate as τ_{max} and f_d decrease, i.e., the time and frequency channel selectivity decreases. Furthermore, for a higher accuracy regarding time and frequency selectivity, one can always increase R and Q respectively.

III. Parallel Equalization at the Receiver

We here extend the proposed receiver structure of [26], [27] to doubly selective channels. Let us consider that the receiver uses $(R+1)(Q+1)$ AFB's working in parallel on the received signal, as shown in Fig. 2. Each AFB has a different index pair (q,r) with $q=0,\ldots,Q$ and $r=0,\ldots,R$ and uses $g^{(q,r)}[n]$ as prototype pulse. After the $(R+1)(Q+1)$ parallel AFB's, the signals coming from each AFB are first equalized and then combined to cancel the distortion caused by the channel selectivity. To formalize this new receiver structure, we need to introduce the following assumption on the per-subcarrier decoding matrices:

$(\mathbf{As3})$ There exists a function $\mathbf{B}(\omega,t)$ such that the per-subcarrier decoding matrices $\mathbf{B}_{m,l}$ at subcarrier m and multicarrier symbol l result from the evaluation of $\mathbf{B}(\omega,t)$ at frequency $\omega=\omega_m$ and time $t=t_l$. We define $\mathbf{B}(\omega,t)$ as

$$\mathbf{B}(\omega,t) = \left(\mathbf{H}(\omega,t)^H\mathbf{H}(\omega,t)\right)^{-1}\mathbf{H}(\omega,t)^H.$$

and its derivatives with respect to time and frequency as

$$\mathbf{B}_{m,l}^{(q,r)} = \frac{d^q}{d\omega^q}\frac{d^r}{dt^r}\mathbf{B}(\omega,t)\Big|_{\omega=\omega_m,t=t_l}.$$

Note that $\mathbf{B}_{m,l}^{(0,0)}=\mathbf{B}_{m,l}$.

The following results can be extended to equalizers that do not invert the channel. However, we restricted the analysis to this case for the sake of compactness of the results and readability of the paper.

Let us denote by $\mathbf{z}_{m_0,l_0}(q,r)$ the demodulated symbol at subcarrier m_0 and multicarrier symbol l_0 of the (q,r) AFB, such that $\mathbf{z}_{m_0,l_0}(0,0)=\mathbf{z}_{m_0,l_0}$. The following theorem gives the weights to combine the outputs of the $(R+1)(Q+1)$ parallel AFB's so that the combined equalized symbol is free from the distortion caused by the frequency selectivity up to an error term, the magnitude of which depends on Q and R.

Theorem III.1. *Under* $(\mathbf{As1})$-$(\mathbf{As3})$*, the demodulated symbols* $\mathbf{z}_{m_0,l_0}(q,r)$ *of each AFB are combined into the symbol*

This article has been accepted for publication in a future issue of this journal, but has not been fully edited. Content may change prior to final publication. Citation information: DOI 10.1109/TSP.2017.2711534, IEEE Transactions on Signal Processing

TABLE II
IMPLEMENTATION COMPLEXITY OF THE DIFFERENT RECEIVERS UNDER COMPARISON.

Considered system	Real-valued multiplications
Classical FBMC ($Q = R = 0$)	$2MN_R(\log_2(2M) + 2\kappa + 2N_T - 3) + 4N_R$
Parallel equalization	$(2MN_R(\log_2(2M) + 2\kappa + 2N_T - 3) + 4N_R)(Q+1)(R+1)$
CP-OFDM	$N_R M(\log_2(2M) + 4N_T - 3) + 2N_R$

$\mathbf{x}_{m_0,l_0}^{(Q,R)}$ *in the following way*

$$\begin{aligned}\mathbf{x}_{m_0,l_0}^{(Q,R)} &= \sum_{r=0}^{R}\sum_{q=0}^{Q} \frac{\jmath^q}{(2M)^q q!(\tilde{N}_s)^r r!}\mathbf{B}_{m_0,l_0}^{(q,r)}\mathbf{z}_{m_0,l_0}(q,r) \quad (9)\\ &= \mathbf{y}_{m_0,l_0} + \boldsymbol{\epsilon}_{m_0,l_0}^{\mathbb{C}}\end{aligned}$$

and as $\frac{\tau_{max}}{T} \to 0$ *and* $f_d T \to 0$*, the residual error after parallel processing,* $\boldsymbol{\epsilon}_{m_0,l_0}^{\mathbb{C}} = \mathbf{x}_{m_0,l_0}^{(Q,R)} - \mathbf{y}_{m_0,l_0}$*, is bounded by*

$$\left\|\boldsymbol{\epsilon}_{m_0,l_0}^{\mathbb{C}}\right\| = O\left(\left(\frac{\tau_{max}}{T}\right)^Q\right) + O\left((f_d T)^R\right).$$

Proof. The proof is given in Appendix VI-B. □

As it is classical in FBMC-OQAM systems, to recover the purely real transmitted symbol, the real part of the equalized signal is taken, i.e., $\hat{\mathbf{d}}_{m_0,l_0}^{(Q,R)} = \Re(\mathbf{x}_{m_0,l_0}^{(Q,R)})$. Note that $\hat{\mathbf{d}}_{m_0,l_0}^{(0,0)} = \hat{\mathbf{d}}_{m_0,l_0}$.

Regarding the complexity of implementation of the proposed design, one can check in Fig. 2 that it scales linearly with the number of parallel AFB's. Each parallel stage has its own filterbank and performs a per-subcarrier single-tap decoding. This shows that the complexity is about $(Q+1)(R+1)$ times the complexity of the classical FBMC-OQAM design. Table II shows the comparison of complexity of the classical designs, the proposed equalization structure and a similar CP-OFDM system, in terms of real-valued multiplications. For the calculation, we assume that the number of subcarriers is a power of two and that an FFT/IFFT of size $2M$ requires $2M(\log_2(2M) - 3) + 4$ real-valued multiplications using the split-radix algorithm [35]. Note that each parallel AFB can be efficiently implemented by the combination of a $2M$-FFT and a polyphase network [36].

We have proposed here a parallel equalization structure at the receiver side. A similar approach could be implemented at the transmitter side, in order to implement a precoder robust to time and frequency selectivity, as was done in [27] for the frequency selective case only.

A. Error model for the residual distortion after parallel processing

The next theorem proposes a model for the residual distortion power after parallel processing, equalization and real part conversion, which correlation matrix is defined as

$$\begin{aligned}\mathbf{P}_{m_0,l_0|H}^{d,(Q,R)} &= \mathbb{E}\left(\left(\mathbf{d}_{m_0,l_0} - \hat{\mathbf{d}}_{m_0,l_0}^{(Q,R)}\right)\left(\mathbf{d}_{m_0,l_0} - \hat{\mathbf{d}}_{m_0,l_0}^{(Q,R)}\right)^T\right)\\ &= \mathbb{E}\left(\Re\left(\boldsymbol{\epsilon}_{m_0,l_0}^{\mathbb{C}}\right)\left(\Re\left(\boldsymbol{\epsilon}_{m_0,l_0}^{\mathbb{C}}\right)\right)^T\right)\end{aligned}$$

where the expectation is taken over the transmitted symbols, for one specific channel realization[2]. Note that $\mathbf{P}_{m_0,l_0|H}^{d,(Q,R)}$ is a $N_T \times N_T$ error correlation matrix. The distortion associated to the k-th stream is given by its k-th diagonal element while its trace gives the total distortion of all streams.

Theorem III.2. *Under* $(\mathbf{As1})$-$(\mathbf{As3})$ *and up to an error term, we can write that*

$$\begin{aligned}&\mathbf{P}_{m_0,l_0|H}^{d,(Q,R)} \quad (10)\\ &= \frac{\eta_{(0,R+1),(0,R+1)}}{\left((R+1)!(\tilde{N}_s)^{R+1}\right)^2}\left(\mathbf{B}^{(0,R+1)}\mathbf{H}\right)\left(\mathbf{B}^{(0,R+1)}\mathbf{H}\right)^H\\ &+ \frac{\eta_{(Q+1,0),(Q+1,0)}}{\left((Q+1)!(2M)^{Q+1}\right)^2}\left(\mathbf{B}^{(Q+1,0)}\mathbf{H}\right)\left(\mathbf{B}^{(Q+1,0)}\mathbf{H}\right)^H\\ &+ \frac{\eta_{(0,R+1),(Q+1,0)}}{(R+1)!(\tilde{N}_s)^{R+1}(Q+1)!(2M)^{Q+1}}\\ &\Big[\Re\left(\left(\mathbf{B}^{(0,R+1)}\mathbf{H}\right)\left(\jmath^{Q+1}\mathbf{B}^{(Q+1,0)}\mathbf{H}\right)^H\right)\\ &\qquad + \Re\left(\left(\jmath^{Q+1}\mathbf{B}^{(Q+1,0)}\mathbf{H}\right)\left(\mathbf{B}^{(0,R+1)}\mathbf{H}\right)^H\right)\Big],\end{aligned}$$

where the different η*'s are pulse related quantities properly defined in the appendix and all frequency-time depending quantities are evaluated at the subcarrier and the multicarrier symbol of interest, i.e.,* $\mathbf{B}^{(0,R+1)} = \mathbf{B}_{m_0,l_0}^{(0,R+1)}, \mathbf{H} = \mathbf{H}_{m_0,l_0}$ *and* $\mathbf{B}^{(Q+1,0)} = \mathbf{B}_{m_0,l_0}^{(Q+1,0)}$.

Proof. The proof is given in Appendix VI-C. □

Theorem III.2 gives a compact approximation for the residual distortion power of a receiver that would use $(R+1)(Q+1)$ parallel AFB's. The approximation is very accurate, as will be shown in the simulations. By inspection of the three terms of $\mathbf{P}_{m_0,l_0|H}^{d,(Q,R)}$, one can see that the first two are related to the distortion caused by time or frequency selectivity respectively while the third term of the sum is a cross term due to the fact that the channel is both selective in time and in frequency. In practice, by evaluating $\mathbf{P}_{m_0,l_0|H}^{d,(Q,R)}$, the receiver could make the best choice of R and Q by trading-off complexity and performance.

Note that the particularization of $\mathbf{P}_{m_0,l_0|H}^{d,(Q,R)}$ to $Q = 0, R = 0$ gives the expression of the distortion associated with the classical FBMC demodulator of Fig. 1 using only one AFB. These results are important to develop link abstraction model for FBMC system-level simulators, as was done in [28]–[30] but under a quasi-static assumption of the channel. Moreover, by particularizing the channel model, the performance analysis

[2]To highlight that the expectation is taken conditionally to the channel realization, we added the subscript $|H$ in the notation $\mathbf{P}_{m_0,l_0|H}^{d,(Q,R)}$.

This article has been accepted for publication in a future issue of this journal, but has not been fully edited. Content may change prior to final publication. Citation information: DOI 10.1109/TSP.2017.2711534, IEEE Transactions on Signal Processing

of an FBMC system with errors of synchronization can be performed, such as carrier frequency offset or timing offset.

B. Noise effect

In the previous analysis, the effect of the noise was discarded. Given that it is assumed uncorrelated with the data samples, its effect can be analyzed independently. If the receive antennas are corrupted by additive circularly-symmetric white Gaussian noise samples $\mathbf{w}[n]$, with zero mean and variance N_0, the received signal can be written as

$$\mathbf{r}_{wn}[n] = \mathbf{r}[n] + \mathbf{w}[n],$$

where the expression of $\mathbf{r}[n]$ is given in (1). The noise samples after the AFB using $g^{(q,r)}[n]$ as prototype filter are given by

$$\mathbf{w}_{m_0,l_0}(q,r) = \sum_{n=0}^{2M\kappa-1} g^{(q,r)*}_{m_0,l_0}[n]\mathbf{w}[n],$$

such that, after parallel combining, the noise samples become

$$\mathbf{w}^{(Q,R)}_{m_0,l_0} = \sum_{r=0}^{R}\sum_{q=0}^{Q} \frac{\jmath^q}{(2M)^q q!(\tilde{N}_s)^r r!}\mathbf{B}^{(q,r)}_{m_0,l_0}\mathbf{w}_{m_0,l_0}(q,r).$$

Then, the real part is taken such that the noise correlation matrix is

$$\mathbf{P}^{wn,(Q,R)}_{m_0,l_0|H} = \mathbb{E}\left(\Re\left(\mathbf{w}^{(Q,R)}_{m_0,l_0}\right)\left(\Re\left(\mathbf{w}^{(Q,R)}_{m_0,l_0}\right)\right)^T\right),$$

where the expectation is taken over the noise statistics, for one specific channel realization. $\mathbf{P}^{wn,(Q,R)}_{m_0,l_0|H}$ is a $N_T \times N_T$ matrix, which k-th diagonal entry corresponds to the noise power associated to stream k. The following theorem gives the expression of $\mathbf{P}^{wn,(Q,R)}_{m_0,l_0|H}$.

Theorem III.3. *The noise correlation matrix after parallel processing is given by*

$$\mathbf{P}^{wn,(Q,R)}_{m_0,l_0|H} = \frac{N_0}{2}\sum_{r'=0}^{R}\sum_{r=0}^{R}\sum_{q=0}^{Q}\sum_{q'=0}^{Q} \frac{(-1)^{q'}\alpha^{(q,r,q',r')}\Re\left(\jmath^{q+q'}\mathbf{B}^{(q,r)}_{m_0,l_0}\mathbf{B}^{(q',r')H}_{m_0,l_0}\right)}{(2M)^{q+q'}q!q'!(\tilde{N}_s)^{r+r'}r!r'!},$$

where

$$\alpha^{(q,r,q',r')} = \sum_{n=0}^{2M\kappa-1} g^{(q,r)}[n]g^{(q',r')}[n].$$

Due to the symmetry of the pulse $g[n]$, the evaluation of the noise can be greatly simplified by using the fact that $\alpha^{(q,r,q',r')} = 0$ if $q+r \neq q'+r' \bmod 2$ ($g^{(q,r)}[n]$ and $g^{(q',r')}[n]$ do not share the same type of symmetry).

Proof. The proof is given in Appendix VI-D. □

This expression is exact and not an approximation as opposed to previous results.

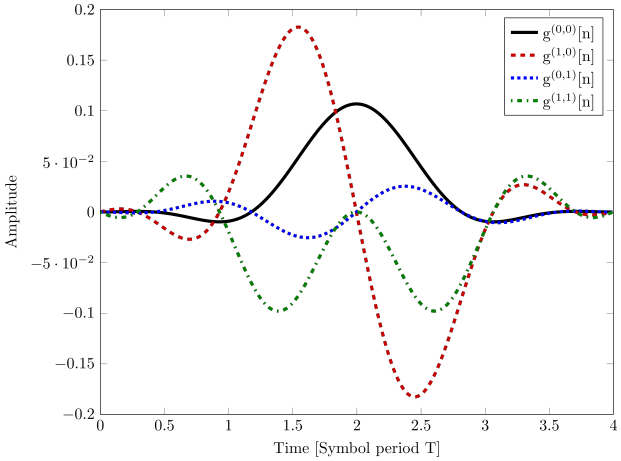

Fig. 3. The prototype pulse and its derivatives used in the simulations.

IV. Simulation Results

This section aims at assessing the performance of the proposed designs and approximations through simulations. Most results of previous sections show that the accuracy of the approximations depend on quantities $\frac{\tau_{max}}{T}$ and Tf_d. We will show in the following that, even for high time and frequency channel selectivity, the symbol period T can be considered large enough with respect to τ_{max} and small with respect to f_d such that the assumption holds and the approximations closely match the simulations results.

Hereby, we assume that the symbol period and subcarrier spacing are fixed to $T = 66,67\mu s$ and 15 kHz, as in LTE systems. The number of real multicarrier symbols is $2N_s = 1000$ and the number of subcarriers is $2M = 128$. The carrier frequency is fixed to $f_c = 2000$ MHz, which corresponds to the E-UTRA band 23. We consider a terminal moving at speed $V = 400$ km/h, which corresponds to a maximal Doppler shift of $f_d = \frac{f_c V}{c} \approx 741$ Hz where c is the speed of light. To characterize the power delay profile of the channel, we will use the 3GPP - Hilly Terrain model [37], which corresponds to a highly frequency selective channel. The ITU - Veh. A channel model will also be used in one figure as an example of mildly frequency selective channel. Note that for both channel models, the Doppler spectrum of each tap is characterized by a classical Jakes model.

The per-stream signal-to-noise-and-distortion ratio (SNDR) is defined as

$$\mathrm{SNDR}_{m,l|H}(k) = \frac{P_s/2}{[\mathbf{P}^{d,(Q,R)}_{m_0,l_0|H}]_{k,k} + [\mathbf{P}^{wn,(Q,R)}_{m_0,l_0|H}]_{k,k}},$$

where $k = 1,\ldots,N_T$ is the stream index. The SNDR is a very useful metric in practice since it characterizes the scale of the signal of interest relatively to the power of the additive noise, ICI and ISI. We recall that $\mathbf{P}^{d,(Q,R)}_{m_0,l_0|H}$ and $\mathbf{P}^{wn,(Q,R)}_{m_0,l_0|H}$ come from computing the expectation with respect to the transmitted symbols and noise for a specific channel realization. The signal-to-noise ratio (SNR) is defined as $\mathrm{SNR} = P_s/N_0$.

In the following simulations, the prototype pulse at transmit and receive sides is the PHYDYAS filter [38] with overlapping factor $\kappa = 4$. The pulse and its first derivatives are shown in Fig. 3.

This article has been accepted for publication in a future issue of this journal, but has not been fully edited. Content may change prior to final publication. Citation information: DOI 10.1109/TSP.2017.2711534, IEEE Transactions on Signal Processing

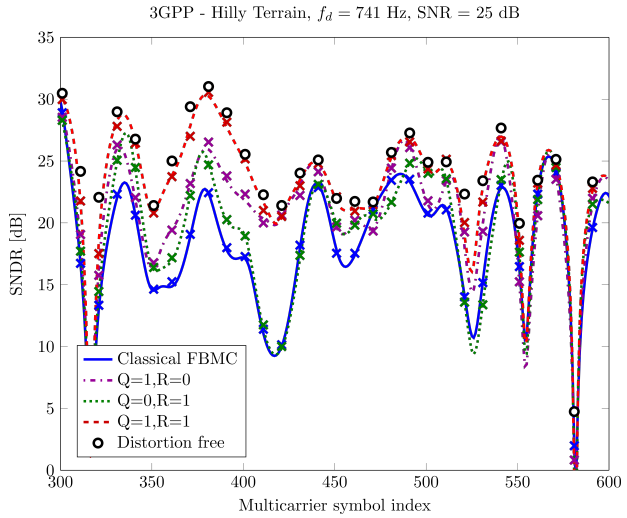

Fig. 4. SNDR at one subcarrier as a function of the multicarrier symbol index and for one SISO channel realization. The simulated performance of the proposed receivers, plotted with crosses, is very close from the lines that represent the proposed SNDR approximation.

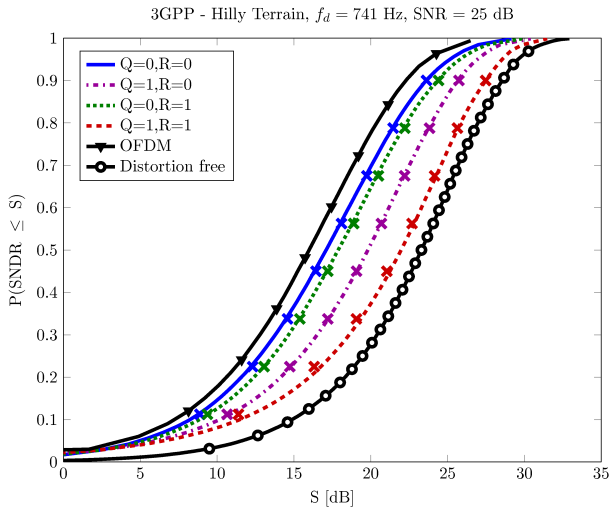

Fig. 5. CDF of the SNDR for different types of parallel receiver structure in the SISO case, for one channel realization. The simulated performance of the proposed receivers, plotted with crosses, is very close from the lines that represent the proposed SNDR approximation. The simulated performance of a CP-OFDM system is also shown.

Furthermore, the performance of a CP-OFDM system is also shown in several figures as a reference. For the sake of comparison, the same number of subcarriers $2M$, the same bandwidth and the same frame duration were considered as in the FBMC case. The cyclic prefix length used here is 10 samples, as it is defined for the first OFDM symbol of each slot in the normal mode of the LTE standard. Hence, for the same frame duration, less information bits are transmitted and the CP-OFDM system has a lower throughput rate than the corresponding FBMC system. Perfect channel estimation was also considered and the decoding matrices at each subcarrier were chosen as the pseudo-inverse of the channel evaluated at that frequency and multicarrier symbol, i.e., zero-forcing equalization.

A. Validation of the theoretic expressions of Theorems III.2 and III.3

In Fig. 4, we consider a SISO case, i.e., $N_R = N_T = 1$ and only one channel realization. For this channel realization, we plotted the SNDR at one subcarrier as a function of time, expressed in terms of the multicarrier symbol index, and for a fixed SNR of 25 dB. We used a high SNR regime to highlight the gain of the proposed designs. Indeed, at low SNR's, the distortion power is negligible compared to the noise power. Different versions of the proposed designs are plotted together with the classical FBMC implementation having only one AFB, as depicted in Fig. 1. The $Q = 0, R = 1$ (resp. $Q = 1, R = 0$) receiver has a second AFB which is used to cancel the first order of the distortion due to time (resp. frequency) selectivity. The $Q = 1, R = 1$ receiver uses four AFB's. The theoretical performance of a distortion free system is also shown, which corresponds to the theoretical case of a perfectly flat channel at the subcarrier level and during the pulse duration, i.e., $\mathbf{H}_{m_0,l_0}^{(q,r)} = \mathbf{0}$ for $q > 0$ or $r > 0$. In other words, only additive noise impacts the equalized symbols. Furthermore, the crosses correspond to the simulated SNDR while the lines (continuous and dashed) correspond to the theoretical SNDR values from Theorems III.2 and III.3.

One can first notice in Fig. 4 the close match between the lines and the crosses, which imply that the proposed expressions of Theorems III.2 and III.3 are very accurate. There is visible gain of the proposed designs with respect to classical FBMC implementation. The $Q = 1, R = 1$ curve is even very close to the distortion free curve. At a few points however, we can see that the classical FBMC receiver performs better than the $Q = 0, R = 1$ and $Q = 1, R = 0$ designs. This is in accordance with the theoretical expression of $P_d(m_0, l_0)$ and is more specifically related to the third term of (10), which is not restricted to be positive and may decrease the distortion, depending on the value of $\eta_{(0,R+1),(Q+1,0)}$. Still, we will see in the next figure that the proposed designs perform better "statistically", looking at their cumulative density functions (CDF).

For the same channel realization as in Fig. 4, Fig. 5 shows the CDF of the SNDR, evaluated at all subcarriers and multicarrier symbols[3]. Again, one can note the close match between the lines (continuous and dashed) and the crosses, demonstrating the accuracy of Theorems III.2 and III.3. Next, increasing the number of AFB's is in each case statistically beneficial. The $Q = 1, R = 1$ curve gets close to the theoretical distortion free curve. To be even closer, it is possible to increase the number of AFB's, at the price of a higher receiver complexity. Furthermore, the performance of a CP-OFDM system is also shown, which is outperformed by all FBMC receivers. Indeed, since the length of the cyclic prefix is much smaller than the channel delay spread, CP-OFDM strongly suffers from the channel frequency selectivity. Furthermore, the bad time-frequency localization of the rectangular pulse in OFDM makes it very sensitive to time selectivity as well [39].

[3]As a reminder, the SNDR metric come from taking the expectation with respect to the statistics of the noise and the transmitted symbols, conditionally to the channel realization.

This article has been accepted for publication in a future issue of this journal, but has not been fully edited. Content may change prior to final publication. Citation information: DOI 10.1109/TSP.2017.2711534, IEEE Transactions on Signal Processing

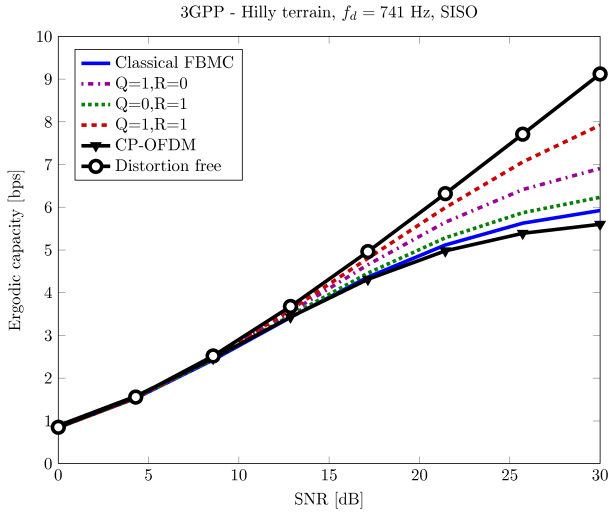

Fig. 6. Ergodic capacity comparison of the proposed different parallel receivers, classical FBMC receiver and CP-OFDM system.

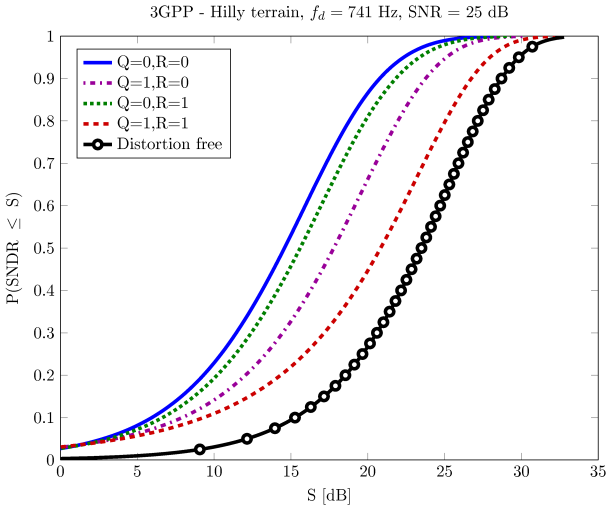

Fig. 8. CDF of the SNDR for different types of parallel receiver structure in the $N_R = N_T = 2$ MIMO case.

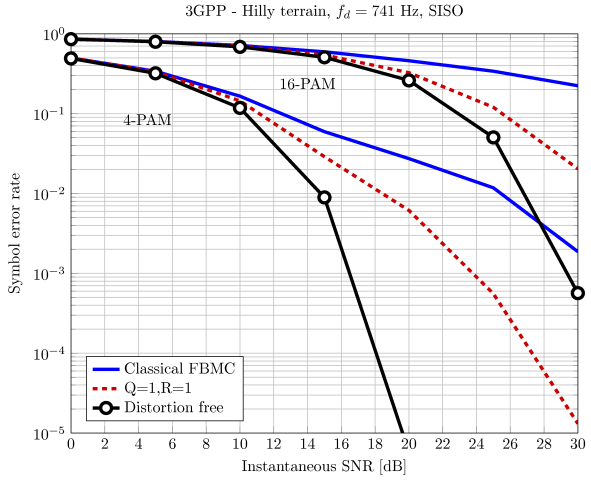

Fig. 7. SER of the classical FBMC system, the proposed $Q = 1, R = 1$ design and the distortion free curve.

One can also see that the $Q = 0, R = 1$ design performs worse than the $Q = 1, R = 0$. This is due to the fact that the channel is comparatively more frequency selective than time selective. This is also related to the choice of the LTE symbol duration T, which is relatively low and provides high robustness to channel time variations. If it was chosen to be larger, the system would be more sensitive to time selectivity and less to frequency selectivity. The authors in [24], [40] provide a detailed performance analysis on the choice of the symbol duration as a function of the channel delay and Doppler spread.

B. Ergodic capacity and outage symbol error rate for random channels

In Fig. 6, the ergodic capacity as a function of the SNR is plotted for the different designs under comparison, in the SISO case and averaged over multiple channel realizations. The distortion plus noise distribution at one subcarrier and multicarrier symbol, for one specific channel realization is approximated by a Gaussian distribution.The ergodic capacity is defined as

$$\mathrm{R} = \mathbb{E}_H \left(\frac{1}{2M2N_s} \sum_{l=0}^{2N_s-1} \sum_{m=0}^{2M-1} \log_2 \left(1 + \mathrm{SNDR}_{m,l|H}(1)\right) \right),$$

expressed in bits per symbol and where the expectation $\mathbb{E}_H$ is taken over the channel statistics. As could be expected, the proposed designs provide more robustness to channel selectivity. Furthermore, CP-OFDM exhibits the worst performance. In Fig. 7, the uncoded SER is plotted as a function of the instantaneous SNR for the classical FBMC system, the proposed $Q = 1, R = 1$ design and the distortion free curve. The instantaneous SNR is defined as the SNR at one particular subcarrier and multicarrier symbol, taking the channel gain into account. The curves are obtained by considering average SNR ranging from 0 to 30 dB and computing for each channel realization, each subcarrier and each multicarrier symbol, the corresponding instantaneous SNR. We plotted the results for a 4-PAM and a 16-PAM constellation sizes. Again, the proposed design outperforms the classical FBMC receiver.

C. Multiple-antenna case

In Fig. 8, the CDF of the SNDR's of the proposed designs evaluated at each subcarrier and multicarrier symbol is plotted for the MIMO case $N_R = N_T = 2$, for a fixed SNR of 25 dB and for multiple channel realizations. The same conclusion as in the SISO case holds. Note that the simulations of all figures were realized for a 3GPP-Hilly Terrain channel model and a maximal Doppler frequency $f_d = 741$ Hz, which corresponds to a channel highly selective both in time and frequency. The results demonstrated the superiority of the receiver structure $Q = 1, R = 1$. However, if the channel was for instance higly time selective but only slightly frequency selective, there would be no large gains of increasing Q to one. To illustrate this, we plotted in Fig. 9 the performance of the same system for the ITU - Veh. A channel model and for the same maximal Doppler frequency, i.e., a channel which is strongly time selective but mildly frequency selective. As one can see, the

This article has been accepted for publication in a future issue of this journal, but has not been fully edited. Content may change prior to final publication. Citation information: DOI 10.1109/TSP.2017.2711534, IEEE Transactions on Signal Processing

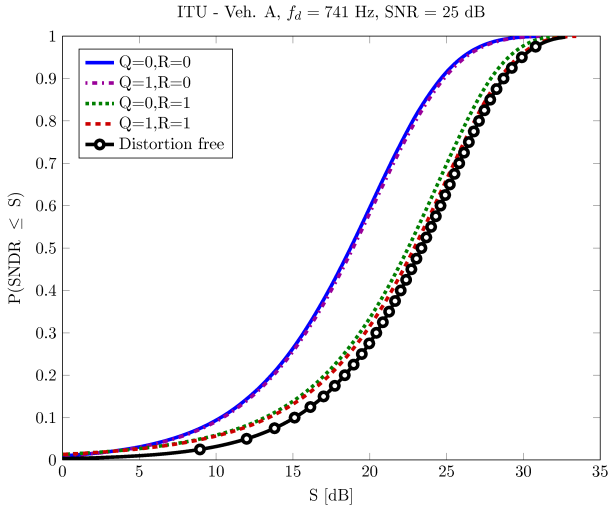

Fig. 9. CDF of the SNDR for different types of parallel receiver structure in the $N_R = N_T = 2$ MIMO case. The channel is strongly time selective and mildly frequency selective.

$Q = 1, R = 1$ and $Q = 0, R = 1$ curves are very close to the distortion free curve.

V. Conclusions

We investigated the effect of time and frequency selectivity on the performance of a FBMC-OQAM system. As the channel becomes more selective in the time-frequency plane, the demodulated symbol are affected by distortion caused by ICI and ISI. A new parallel equalization structure was proposed, such that the performance of a distortion free system can be retrieved by the use of multiple AFB's at the receiver side. A theoretical approximation of the residual distortion and noise powers after equalization was derived. The accuracy of the approximation as well as the performance of the proposed equalization structure were validated through simulations in the single-antenna and multiple-antenna cases.

VI. Appendix

A. Proof of Proposition II.1

Let us rewrite (2) by setting $n' = n - b$ as

$$\begin{aligned}\mathbf{z}_{m_0,l_0} &= \sum_{m,l}\sum_{n'}\sum_{b=0}^{L_b} \boldsymbol{\mathcal{H}}[b,n'+b] g^*_{m_0,l_0}[n'+b]\mathbf{d}_{m,l}p_{m,l}[n'].\\ &= \sum_{m,l}\sum_{n'} \boldsymbol{\Delta}_{m_0,l_0}[n']\mathbf{d}_{m,l}p_{m,l}[n'], \qquad (11)\end{aligned}$$

where we have defined

$$\begin{aligned}\boldsymbol{\Delta}_{m_0,l_0}[n'] &= \sum_{b=0}^{L_b} \boldsymbol{\mathcal{H}}[b,n'+b] g^*_{m_0,l_0}[n'+b]\\ &= \beta^*_{m_0,l_0}\sum_{b=0}^{L_b} \boldsymbol{\mathcal{H}}[b,n'+b] g[n'+b-l_0M] e^{-\jmath\omega_{m_0}b}, \qquad (12)\end{aligned}$$

with $\beta_{m_0,l_0} = \jmath^{l_0+m_0} e^{\jmath\omega_{m_0}(n'-\frac{2M\kappa-1}{2})}$. We are now going to develop the expression of $\boldsymbol{\Delta}_{m_0,l_0}[n']$.

a) Taylor expansion with respect to time variation of the channel: Note that $\boldsymbol{\mathcal{H}}[b,n'+b]$ comes from the evaluation at time $t = \frac{n'+b}{2\tilde{N}_s M}$ of the smooth function $\mathbf{F}_b(t)$ defined by

$$\mathbf{F}_b(t) = \sum_{\nu=-L_\nu}^{L_\nu} \boldsymbol{\Psi}[b,\nu] e^{\jmath 2\pi t\nu},$$

which can be seen as the time variant response of the b-th tap of the channel. We have

$$\boldsymbol{\mathcal{H}}[b,n'+b] = \mathbf{F}_b(t)\big|_{t=\frac{n'+b}{2\tilde{N}_s M}}.$$

Since $\boldsymbol{\mathcal{H}}[b,n'+b]g[n'+b-l_0M]$ is non zero only for $n'+b \in \{l_0M,\ldots,l_0M+2M\kappa-1\}$, let us perform a Taylor expansion of $\mathbf{F}_b(t)$ around time instant $t_{l_0} = \frac{1}{2\tilde{N}_s M}(l_0M + \frac{2M\kappa-1}{2})$ that we evaluate at $t = \frac{n'+b}{2\tilde{N}_s M}$. Note that this Taylor expansion converges for any t since the convergence radius of the exponential function is infinite. We obtain

$$\begin{aligned}\boldsymbol{\mathcal{H}}[b,n'+b] &= \sum_{r=0}^{+\infty} \frac{\mathbf{F}_b^{(r)}(t_{l_0})}{r!}(t-t_{l_0})^r\Big|_{t=\frac{n'+b}{2\tilde{N}_s M}}\\ &= \sum_{r=0}^{+\infty}\sum_{\nu=-L_\nu}^{L_\nu} \frac{(\jmath 2\pi\nu)^r}{(\tilde{N}_s)^r r!}\boldsymbol{\Psi}[b,\nu]e^{\jmath 2\pi t_{l_0}\nu}\\ &\qquad \left(\frac{n'+b-l_0M-\frac{2M\kappa-1}{2}}{2M}\right)^r.\end{aligned}$$

Replacing this expression of $\boldsymbol{\mathcal{H}}[b,n'+b]$ in (12), we obtain

$$\begin{aligned}\boldsymbol{\Delta}_{m_0,l_0}[n'] = \beta^*_{m_0,l_0}\sum_{r=0}^{+\infty}\sum_{\nu=-L_\nu}^{L_\nu} \frac{(\jmath 2\pi\nu)^r}{(\tilde{N}_s)^r r!}e^{\jmath 2\pi t_{l_0}\nu}\\ \sum_{b=0}^{L_b}\boldsymbol{\Psi}[b,\nu]g^{(0,r)}[n'+b-l_0M]e^{-\jmath\omega_{m_0}b}. \qquad (13)\end{aligned}$$

b) Taylor expansion with respect to delayed pulse: Remember that $g^{(0,r)}[n'+b-l_0M]$ can be seen as the evaluation of the function $\tilde{g}^{(0,r)}(t)$ at $\tilde{t} = (n'+b-l_0M-\frac{2M\kappa-1}{2})\frac{1}{2M}$. Let us perform a Taylor expansion of $\tilde{g}^{(0,r)}(t)$ around point $\tilde{t}_{l_0} = (n'-l_0M-\frac{2M\kappa-1}{2})\frac{1}{2M}$ that we evaluate at $\tilde{t}$

$$\begin{aligned}g^{(0,r)}[n'+b-l_0M] &= \sum_{q=0}^{+\infty}\frac{\tilde{g}^{(q,r)}\left(\tilde{t}_{l_0}\right)}{q!}(\tilde{t}-\tilde{t}_{l_0})^q\\ &= \sum_{q=0}^{+\infty}\frac{g^{(q,r)}[n'-l_0M]}{(2M)^q q!}b^q.\end{aligned}$$

Note that, due to $(\mathbf{As2})$, $\tilde{g}(t)$ is analytic and the same holds for $\tilde{g}^{(q,r)}(t)$ since the product and derivatives of analytic functions are also analytic. Hence the above Taylor expansion is ensured to converge to $g^{(0,r)}[n'+b-l_0M]$, which is

This article has been accepted for publication in a future issue of this journal, but has not been fully edited. Content may change prior to final publication. Citation information: DOI 10.1109/TSP.2017.2711534, IEEE Transactions on Signal Processing

bounded. Replacing the expression of $g^{(0,r)}[n'+b-l_0M]$ by its Taylor expansion in (13), we obtain

$$\begin{aligned}\boldsymbol{\Delta}_{m_0,l_0}[n'] &= \beta^*_{m_0,l_0}\sum_{r=0}^{+\infty}\sum_{q=0}^{+\infty}\frac{g^{(q,r)}[n'-l_0M]}{(2M)^q q!(\tilde{N}_s)^r r!}\\ &\quad\sum_{b=0}^{L_b}\sum_{\nu=-L_\nu}^{L_\nu} b^q(\jmath 2\pi\nu)^r\boldsymbol{\Psi}[b,\nu]e^{\jmath 2\pi t_{l_0}\nu}e^{-\jmath\omega_{m_0}b}\\ &\overset{(5)}{=}\sum_{r=0}^{+\infty}\sum_{q=0}^{+\infty}\frac{\jmath^q\mathbf{H}^{(q,r)}_{m_0,l_0}}{(2M)^q q!(\tilde{N}_s)^r r!}g^{(q,r)*}_{m_0,l_0}[n'].\end{aligned}$$

If we replace this expression of $\boldsymbol{\Delta}_{m_0,l_0}[n']$ in (11), we finally obtain

$$\begin{aligned}&\mathbf{z}_{m_0,l_0}\\ &=\sum_{r=0}^{+\infty}\sum_{q=0}^{+\infty}\frac{\jmath^q\mathbf{H}^{(q,r)}_{m_0,l_0}}{(2M)^q q!(\tilde{N}_s)^r r!}\sum_{m,l}\mathbf{d}_{m,l}\sum_{n'}p_{m,l}[n']g^{(q,r)*}_{m_0,l_0}[n']\\ &=\sum_{r=0}^{+\infty}\sum_{q=0}^{+\infty}\frac{\jmath^q}{(2M)^q q!(\tilde{N}_s)^r r!}\mathbf{H}^{(q,r)}_{m_0,l_0}\mathbf{y}^{(q,r)}_{m_0,l_0}. \qquad (14)\end{aligned}$$

The above repeated series can be replaced by a double series, which allows to swap the order of the two indexes q and r. To see this, it is enough to see that the double series is absolutely convergent. Indeed, this can be deduced by looking at the different terms of $\mathbf{z}_{m_0,l_0}$ in (11). First, we have just shown that $\boldsymbol{\Delta}_{m_0,l_0}[n']$ can be replaced by a double series, which converges and remains bounded. Further, the transmitted symbols $\mathbf{d}_{m,l}$ and the energy of the pulse $p[n]$ are bounded by assumption.

c) Bounding the approximation error: The (Q,R)-th order approximation of $\mathbf{z}_{m_0,l_0}$ is given by the truncation of the Taylor expansion to its (Q,R) first terms

$$\mathbf{z}^{(Q,R)}_{m_0,l_0}=\sum_{r=0}^{R}\sum_{q=0}^{Q}\frac{\jmath^q}{(2M)^q q!(\tilde{N}_s)^r r!}\mathbf{H}^{(q,r)}_{m_0,l_0}\mathbf{y}^{(q,r)}_{m_0,l_0}.$$

and the approximation error is

$$\mathbf{z}_{m_0,l_0}-\mathbf{z}^{(Q,R)}_{m_0,l_0}=\sum_{(q,r)\in\Omega}\frac{\jmath^q}{(2M)^q q!(\tilde{N}_s)^r r!}\mathbf{H}^{(q,r)}_{m_0,l_0}\mathbf{y}^{(q,r)}_{m_0,l_0}$$

where Ω denotes the set (q,r) such that $q>Q$ or $r>R$. Using the triangular inequality and the fact that the channel power is bounded, we can write

$$\begin{aligned}\left\|\mathbf{z}_{m_0,l_0}-\mathbf{z}^{(Q,R)}_{m_0,l_0}\right\| &\le \sum_{(r,q)\in\Omega}\frac{\left\|\mathbf{H}^{(q,r)}_{m_0,l_0}\right\|}{(2M)^q(\tilde{N}_s)^r}\left\|\frac{\mathbf{y}^{(q,r)}_{m_0,l_0}}{q!r!}\right\|\\ &\overset{(5)}{\le}\sum_{(r,q)\in\Omega}\sum_{b=0}^{L_b}\sum_{\nu=-L_\nu}^{L_\nu}\left(\frac{b}{2M}\right)^q\left(\frac{2\pi\nu}{\tilde{N}_s}\right)^r\|\boldsymbol{\Psi}[b,\nu]\|\left\|\frac{\mathbf{y}^{(q,r)}_{m_0,l_0}}{q!r!}\right\|.\end{aligned}$$

Since the channel has finite energy, we can bound

$$\sum_{b=0}^{L_b}\sum_{\nu=-L_\nu}^{L_\nu}\|\boldsymbol{\Psi}[b,\nu]\|\le C_{\boldsymbol{\Psi}},$$

and we obtain

$$\begin{aligned}&\left\|\mathbf{z}_{m_0,l_0}-\mathbf{z}^{(Q,R)}_{m_0,l_0}\right\|\\ &\le C_{\boldsymbol{\Psi}}\sum_{(r,q)\in\Omega}\left(\frac{L_b}{2M}\right)^q\left(\frac{2\pi L_\nu}{\tilde{N}_s}\right)^r\left\|\frac{\mathbf{y}^{(q,r)}_{m_0,l_0}}{q!r!}\right\|.\end{aligned}$$

Under $(\mathbf{As1})$, we have $L_b=\lfloor\frac{\tau_{max}2M}{T}\rfloor$ and $L_\nu=\lfloor f_d\tilde{N}_sT\rfloor$. Using the fact that the symbols are bounded, the definition of $\mathbf{y}^{(q,r)}_{m_0,l_0}$ in (6) and under $(\mathbf{As2})$, we can write that, as $\frac{\tau_{max}}{T}\to 0$ and $f_dT\to 0$, we have

$$\left\|\mathbf{z}_{m_0,l_0}-\mathbf{z}^{(Q,R)}_{m_0,l_0}\right\|=O\left(\left(\frac{\tau_{max}}{T}\right)^Q\right)+O\left((f_dT)^R\right),$$

which completes the proof of Proposition II.1.

B. Proof of Theorem III.1

We will begin by showing that the decoder and its derivatives are bounded. Under $(\mathbf{As3})$, we have that $\mathbf{B}(\omega,t)\mathbf{H}(\omega,t)=\mathbf{I}_{N_T}$, which is not dependent on time and frequency and hence

$$\begin{aligned}(\mathbf{B}_{m,l}\mathbf{H}_{m,l})^{(\tilde{q},\tilde{r})} &= \sum_{q=0}^{\tilde{q}}\sum_{r=0}^{\tilde{r}}\binom{\tilde{q}}{q}\binom{\tilde{r}}{r}\mathbf{B}^{(q,r)}_{m,l}\mathbf{H}^{(\tilde{q}-q,\tilde{r}-r)}_{m,l}\\ &=\mathbf{I}_{N_T}\delta[\tilde{q}]\delta[\tilde{r}]. \qquad (15)\end{aligned}$$

We can reason by induction to show that $\sup_{m,l}\|\mathbf{B}^{(q,r)}_{m,l}\|<+\infty$ for each q and r. First, for $q=r=0$, we have

$$\begin{aligned}\sup_{m,l}\|\mathbf{B}_{m,l}\| &\le \sup_{m,l}\|\left(\mathbf{H}^H_{m,l}\mathbf{H}_{m,l}\right)^{-1}\|\sup_{m,l}\|\mathbf{H}^H_{m,l}\|\\ &\le\frac{\sup_{(\omega,t)}\lambda^{1/2}_{\max}\left(\mathbf{H}^H(\omega,t)\mathbf{H}(\omega,t)\right)}{\inf_{(\omega,t)}\lambda_{\min}\left(\mathbf{H}^H(\omega,t)\mathbf{H}(\omega,t)\right)},\end{aligned}$$

which is bounded under $(\mathbf{As1})$. Otherwise, using (15), we have,

$$\begin{aligned}\|\mathbf{B}^{(q,r)}_{m,l}\| &\le \frac{\|\mathbf{B}^{(q,r)}_{m,l}\mathbf{H}_{m,l}\|}{\lambda^{1/2}_{\min}\left(\mathbf{H}^H(\omega,t)\mathbf{H}(\omega,t)\right)}\\ &\le\sum_{\substack{(i,j)=(0,0),\\(i,j)\neq(q,r)}}^{(q,r)}\binom{q}{i}\binom{r}{j}\|\mathbf{B}^{(i,j)}_{m,l}\|\frac{\|\mathbf{H}^{(q-i,r-j)}_{m,l}\|}{\lambda^{1/2}_{\min}\left(\mathbf{H}^H(\omega,t)\mathbf{H}(\omega,t)\right)}\end{aligned}$$

and the result follows from taking the supremum with respect to m,l and applying the induction hypothesis. This concludes the proof that $\sup_{m,l}\|\mathbf{B}^{(q,r)}_{m,l}\|<+\infty$. In the following, we drop the subscript m_0,l_0 for the sake of clarity. Let us define $\alpha=\frac{\tau_{max}}{T}$ and $\beta=f_dT$. Using the result of Proposition II.1, we can write

$$\mathbf{z}(q,r)=\sum_{r_1=0}^{R-r}\sum_{q_1=0}^{Q-q}\frac{\jmath^{q_1}\mathbf{H}^{(q_1,r_1)}}{(2M)^{q_1}q_1!(\tilde{N}_s)^{r_1}r_1!}\mathbf{y}^{(q+q_1,r+r_1)}+\boldsymbol{\epsilon}(q,r)$$

where $\|\boldsymbol{\epsilon}(q,r)\|=O\left(\alpha^{Q-q}\right)+O\left(\beta^{R-r}\right)$. Using the definition of $\mathbf{x}^{(Q,R)}$ in (9), we can write

$$\begin{aligned}&\mathbf{x}^{(Q,R)}\\ &=\sum_{r=0}^{R}\sum_{q=0}^{Q}\sum_{r_1=0}^{R-r}\sum_{q_1=0}^{Q-q}\frac{\jmath^{q+q_1}\mathbf{B}^{(q,r)}\mathbf{H}^{(q_1,r_1)}\mathbf{y}^{(q+q_1,r+r_1)}}{(2M)^{q+q_1}q_1!q!(\tilde{N}_s)^{r+r_1}r!r_1!}+\boldsymbol{\epsilon}^{\mathbb{C}},\end{aligned}$$

This article has been accepted for publication in a future issue of this journal, but has not been fully edited. Content may change prior to final publication. Citation information: DOI 10.1109/TSP.2017.2711534, IEEE Transactions on Signal Processing

where the error $\boldsymbol{\epsilon}^{\mathbb{C}}$ is given by

$$\begin{aligned}\boldsymbol{\epsilon}^{\mathbb{C}} &= \sum_{r=0}^{R}\sum_{q=0}^{Q}\frac{\jmath^q}{(2M)^q q!(\tilde{N}_s)^r r!}\mathbf{B}^{(q,r)}\boldsymbol{\epsilon}(q,r)\\ &= O\left(\alpha^Q\right)+O\left(\beta^R\right),\end{aligned}$$

where we used the fact that $\sup_{m,l}\|\mathbf{B}_{m,l}^{(q,r)}\|<+\infty$ and $\frac{1}{2M}\leq\frac{L_b}{2M}\leq\frac{\tau_{max}}{T}$ and $\frac{1}{\tilde{N}_s}\leq\frac{L_\nu}{\tilde{N}_s}\leq f_dT$. Let us take $\tilde{q}=q+q_1$ and $\tilde{r}=r+r_1$, $\mathbf{x}^{(Q,R)}$ can be rewritten as

$$\begin{aligned}&\mathbf{x}^{(Q,R)}-\boldsymbol{\epsilon}^{\mathbb{C}}\\ &=\sum_{r=0}^{R}\sum_{q=0}^{Q}\sum_{\tilde{r}=r}^{R}\sum_{\tilde{q}=q}^{Q}\frac{\jmath^{\tilde{q}}\mathbf{B}^{(q,r)}\mathbf{H}^{(\tilde{q}-q,\tilde{r}-r)}\mathbf{y}^{(\tilde{q},\tilde{r})}}{r!q!(\tilde{r}-r)!(\tilde{q}-q)!(2M)^{\tilde{q}}(\tilde{N}_s)^{\tilde{r}}}\\ &=\sum_{\tilde{r}=0}^{R}\sum_{\tilde{q}=0}^{Q}\frac{\jmath^{\tilde{q}}}{\tilde{q}!(2M)^{\tilde{q}}\tilde{r}!(\tilde{N}_s)^{\tilde{r}}}\sum_{q=0}^{\tilde{q}}\sum_{r=0}^{\tilde{r}}\frac{\mathbf{B}^{(q,r)}\mathbf{H}^{(\tilde{q}-q,\tilde{r}-r)}\mathbf{y}^{(\tilde{q},\tilde{r})}}{r!q!(\tilde{r}-r)!(\tilde{q}-q)!}.\end{aligned}$$

Using the identity in (15), we finally find that $\mathbf{x}^{(Q,R)}=\mathbf{y}+\boldsymbol{\epsilon}^{\mathbb{C}}$, which completes the proof.

C. Proof of Theorem III.2

Using Theorem III.1, we have[4]

$$\mathbf{x}^{(Q+1,R+1)}=\sum_{r=0}^{R+1}\sum_{q=0}^{Q+1}\frac{\jmath^q}{(2M)^q q!(\tilde{N}_s)^r r!}\mathbf{B}^{(q,r)}\mathbf{z}(q,r)$$

and $\left\|\mathbf{x}^{(Q+1,R+1)}-\mathbf{y}\right\|=O\left(\alpha^{Q+1}\right)+O\left(\beta^{R+1}\right)$. Note that,

$$\begin{aligned}&\mathbf{x}^{(Q+1,R+1)}-\mathbf{y}=\mathbf{x}^{(Q,R)}-\mathbf{y}+\frac{\jmath^{Q+1}\mathbf{B}^{(Q+1,0)}\mathbf{z}(Q+1,0)}{(2M)^{Q+1}(Q+1)!}\\ &+\frac{\mathbf{B}^{(0,R+1)}\mathbf{z}(0,R+1)}{(\tilde{N}_s)^{R+1}(R+1)!}+\sum_{r=1}^{R+1}\frac{\jmath^{Q+1}\mathbf{B}^{(Q+1,r)}\mathbf{z}(Q+1,r)}{(2M)^{Q+1}(Q+1)!(\tilde{N}_s)^r r!}\\ &+\sum_{q=1}^{Q}\frac{\jmath^q\mathbf{B}^{(q,R+1)}\mathbf{z}(q,R+1)}{(2M)^q q!(\tilde{N}_s)^{R+1}(R+1)!}.\end{aligned}$$

Combining the two previous equations, we can write the following approximation of the residual distortion

$$\begin{aligned}&\boldsymbol{\epsilon}^{\mathbb{C}}=\mathbf{x}^{(Q,R)}-\mathbf{y}\\ &=-\frac{\jmath^{Q+1}\mathbf{B}^{(Q+1,0)}\mathbf{z}(Q+1,0)}{(2M)^{Q+1}(Q+1)!}-\frac{\mathbf{B}^{(0,R+1)}\mathbf{z}(0,R+1)}{(\tilde{N}_s)^{R+1}(R+1)!}+\boldsymbol{\epsilon}_1,\end{aligned}$$

where $\boldsymbol{\epsilon}_1$ is the error on the approximation of the residual distortion itself, which can be bounded as

$$\begin{aligned}\|\boldsymbol{\epsilon}_1\|&\leq\left\|\sum_{r=1}^{R+1}\frac{\jmath^{Q+1}\mathbf{B}^{(Q+1,r)}\mathbf{z}(Q+1,r)}{(2M)^{Q+1}(Q+1)!(\tilde{N}_s)^r r!}\right\|\\ &+\left\|\sum_{q=1}^{Q}\frac{\jmath^q\mathbf{B}^{(q,R+1)}\mathbf{z}(q,R+1)}{(2M)^q q!(\tilde{N}_s)^{R+1}(R+1)!}\right\|\\ &+O\left(\alpha^{Q+1}\right)+O\left(\beta^{R+1}\right)\\ &=O\left(\alpha^Q\beta\right)+O\left(\alpha\beta^R\right)+O\left(\alpha^{Q+1}\right)+O\left(\beta^{R+1}\right),\end{aligned}$$

[4]Here again, we dropped the subscript m_0,l_0 for the sake of clarity.

where we used the same bounding methodology as in Appendices VI-A and VI-B. Then, we can write, using the result of Proposition II.1,

$$\begin{aligned}\boldsymbol{\epsilon}^{\mathbb{C}}&=-\frac{\jmath^{Q+1}\mathbf{B}^{(Q+1,0)}\mathbf{H}\mathbf{y}^{(Q+1,0)}}{(2M)^{Q+1}(Q+1)!}-\frac{\mathbf{B}^{(0,R+1)}\mathbf{H}\mathbf{y}^{(0,R+1)}}{(\tilde{N}_s)^{R+1}(R+1)!}+\boldsymbol{\epsilon}_2 \qquad (16)\\ \|\boldsymbol{\epsilon}_2\|&=O\left(\alpha^Q\beta\right)+O\left(\alpha\beta^R\right)+O\left(\alpha^{Q+1}\right)+O\left(\beta^{R+1}\right).\end{aligned}$$

We now need to compute $\mathbf{P}_{m_0,l_0|H}^{d,(Q,R)}=\mathbb{E}\left(\Re\left(\boldsymbol{\epsilon}^{\mathbb{C}}\right)\left(\Re\left(\boldsymbol{\epsilon}^{\mathbb{C}}\right)\right)^T\right)$. To do this, we need to define some pulse-related quantities. Given two generic pulses, p,q of length $2M\kappa$, let $\mathbf{P}$ and $\mathbf{Q}$ denote two $2M\times\kappa$ matrices obtained by arranging the samples of the respective pulses in columns from left to right. We will define

$$\begin{aligned}\mathcal{R}(p,q)&=\mathbf{P}\circledast\mathbf{J}_{2M}\mathbf{Q}\\ \mathcal{S}(p,q)&=(\mathbf{J}_2\otimes\mathbf{I}_M)\,\mathbf{P}\circledast\mathbf{J}_{2M}\mathbf{Q},\end{aligned}$$

where $\circledast$ denotes row-wise convolution, $\otimes$ denotes Kronecker product, $\mathbf{I}_M$ (resp. $\mathbf{J}_M$) are the identity (resp. exchange) matrices of order M. Given four generic pulses p,q,r,s, we define

$$\begin{aligned}&\eta^{\pm}(p,q,r,s)\\ &=\frac{P_sM}{2}\mathrm{tr}\left[\mathbf{U}^{+}\mathcal{R}(p,q)\,\mathcal{R}^T(r,s)+\mathbf{U}^{-}\mathcal{S}(p,q)\,\mathcal{S}^T(r,s)\right]\\ &\eta^{\mp}(p,q,r,s)\\ &=\frac{P_sM}{2}\mathrm{tr}\left[\mathbf{U}^{-}\mathcal{R}(p,q)\,\mathcal{R}^T(r,s)+\mathbf{U}^{+}\mathcal{S}(p,q)\,\mathcal{S}^T(r,s)\right],\end{aligned}$$

where $\mathbf{U}^{\pm}=\mathbf{I}_2\otimes(\mathbf{I}_M\pm\mathbf{J}_M)$. In order to simplify the notations and since the pulse at the transmit side always is p and the pulse at the receiver is a derivative of g, given four integers q_1,r_1,q_2,r_2, we will define $\eta^{(+,-)}_{(q_1,r_1),(q_2,r_2)}=\eta^{\pm}\left(p,g^{(q_1,r_1)},p,g^{(q_2,r_2)}\right)$.

We can now obtain an expression of the residual distortion by using the fact that, under $((\mathbf{As2}))$ [26, Appendix B] and neglecting tail effects,

$$\begin{aligned}\mathbb{E}\left(\Re(\mathbf{y}^{(q_1,r_1)})\Re^T(\mathbf{y}^{(q_2,r_2)})\right)&=\eta^{(+,-)}_{(q_1,r_1),(q_2,r_2)}\mathbf{I}_{N_T},\\ \mathbb{E}\left(\Im(\mathbf{y}^{(q_1,r_1)})\Im^T(\mathbf{y}^{(q_2,r_2)})\right)&=\eta^{(-,+)}_{(q_1,r_1),(q_2,r_2)}\mathbf{I}_{N_T},\\ \mathbb{E}\left(\Re(\mathbf{y}^{(q_1,r_1)})\Im^T(\mathbf{y}^{(q_2,r_2)})\right)&=\mathbf{0}.\end{aligned}$$

The resulting expression can be simplified using [41, Lemma 3] showing that, in the particular case considered here, we have $\eta^{(+,-)}_{(q_1,r_1),(q_2,r_2)}=\eta^{(-,+)}_{(q_1,r_1),(q_2,r_2)}$ (the transmit pulse does not change). Hence, we will omit the superscripts $^{(+,-)}$ and $^{(-,+)}$. The result of Theorem III.2 is then found by computing $\mathbf{P}_{m_0,l_0|H}^{d,(Q,R)}=\mathbb{E}\left(\Re\left(\boldsymbol{\epsilon}^{\mathbb{C}}\right)\left(\Re\left(\boldsymbol{\epsilon}^{\mathbb{C}}\right)\right)^T\right)$ with the expression of $\boldsymbol{\epsilon}^{\mathbb{C}}$ given in (16) (neglecting the error term $\boldsymbol{\epsilon}_2$) and using the above definition of $\eta_{(q_1,r_1),(q_2,r_2)}$.

This article has been accepted for publication in a future issue of this journal, but has not been fully edited. Content may change prior to final publication. Citation information: DOI 10.1109/TSP.2017.2711534, IEEE Transactions on Signal Processing

D. Proof of Theorem III.3

Let us develop the expression of $\mathbf{P}^{wn,(Q,R)}_{m_0,l_0|H}$,

$$\mathbf{P}^{wn,(Q,R)}_{m_0,l_0|H} = \mathbb{E}\left(\Re\left(\mathbf{w}^{(Q,R)}_{m_0,l_0}\right)\left(\Re\left(\mathbf{w}^{(Q,R)}_{m_0,l_0}\right)\right)^T\right)$$
$$= \sum_{r'=0}^{R}\sum_{r=0}^{R}\sum_{q=0}^{Q}\sum_{q'=0}^{Q}\frac{1}{(2M)^{q+q'}q!q'!(\tilde{N}_s)^{r+r'}r!r'!}$$
$$\mathbb{E}\left(\Re\left(\jmath^q\mathbf{B}^{(q,r)}_{m_0,l_0}\sum_{n=0}^{2M\kappa-1}g^{(q,r)*}_{m_0,l_0}[n]\mathbf{w}[n]\right)\right.$$
$$\left.\Re\left(\jmath^{q'}\sum_{n'=0}^{2M\kappa-1}g^{(q',r')*}_{m_0,l_0}[n']\mathbf{w}[n']^T\left(\mathbf{B}^{(q',r')}_{m_0,l_0}\right)^T\right)\right)$$

Using the fact that for any complex matrix $\mathbf{A}$, $\Re(\mathbf{A}) = \frac{1}{2}(\mathbf{A}+\mathbf{A}^*)$ and that $\mathbf{w}[n]$ is white and circularly symmetric, $\mathbb{E}(\mathbf{w}[n]\mathbf{w}^T[n']) = \mathbf{0}$ and $\mathbb{E}(\mathbf{w}[n]\mathbf{w}^H[n']) = N_0\mathbf{I}_{N_R}\delta[n-n']$, the expression of $\mathbf{P}^{wn,(Q,R)}_{m_0,l_0|H}$ simplifies to

$$\mathbf{P}^{wn,(Q,R)}_{m_0,l_0|H} = \sum_{r'=0}^{R}\sum_{r=0}^{R}\sum_{q=0}^{Q}\sum_{q'=0}^{Q}\frac{1}{(2M)^{q+q'}q!q'!(\tilde{N}_s)^{r+r'}r!r'!}$$
$$\frac{N_0}{4}\mathrm{tr}\left[\jmath^q(-\jmath)^{q'}\mathbf{B}^{(q,r)}_{m_0,l_0}\left(\mathbf{B}^{(q',r')}_{m_0,l_0}\right)^H\sum_{n=0}^{2M\kappa-1}g^{(q,r)*}_{m_0,l_0}[n]g^{(q',r')}_{m_0,l_0}[n]\right.$$
$$\left.+(-\jmath)^q\jmath^{q'}\mathbf{B}^{(q,r)*}_{m_0,l_0}\left(\mathbf{B}^{(q',r')}_{m_0,l_0}\right)^T\sum_{n=0}^{2M\kappa-1}g^{(q,r)}_{m_0,l_0}[n]g^{(q',r')*}_{m_0,l_0}[n]\right].$$

Defining, $\alpha^{(q,r,q',r')} = \sum_{n=0}^{2M\kappa-1}g^{(q,r)*}_{m_0,l_0}[n]g^{(q',r')}_{m_0,l_0}[n] = \sum_{n=0}^{2M\kappa-1}g^{(q,r)}[n]g^{(q',r')}[n]$, we find the expression given in Theorem III.3. Using the fact that $g[n]$ is even or odd and that $g^{(q,r)}[n]$ shares the same type of symmetry as $g[n]$ if $q+r=0 \bmod 2$ and the opposite otherwise, one can easily check that $\alpha^{(q,r,q',r')} \neq 0$ only if $q+r=q'+r' \bmod 2$. This completes the proof.

REFERENCES

[1] B. Farhang-Boroujeny, "OFDM versus filter bank multicarrier," *IEEE Signal Process. Mag.*, vol. 28, no. 3, pp. 92–112, May 2011.

[2] A. Aminjavaheri, A. Farhang, A. RezazadehReyhani, and B. Farhang-Boroujeny, "Impact of timing and frequency offsets on multicarrier waveform candidates for 5G," in *2015 IEEE Signal Processing and Signal Processing Education Workshop (SP/SPE)*, Aug 2015, pp. 178–183.

[3] M. Bellanger, D. Le Ruyet, D. Roviras, M. Terré, J. Nossek, L. Baltar, Q. Bai, D. Waldhauser, M. Renfors, T. Ihalainen *et al.*, "FBMC physical layer: a primer," *PHYDYAS, January*, 2010.

[4] F. Rottenberg, Y. Medjahdi, E. Kofidis, and J. Louveaux, "Preamble-based channel estimation in asynchronous FBMC-OQAM distributed MIMO systems," in *12th International Symposium on Wireless Communication Systems (ISWCS)*, 2015.

[5] T. Ihalainen, T. H. Stitz, M. Rinne, and M. Renfors, "Channel equalization in filter bank based multicarrier modulation for wireless communications," *EURASIP Journal on Applied Signal Processing*, vol. 2007, no. 1, pp. 140–140, 2007.

[6] M. Caus, A. Pérez-Neira *et al.*, "Transmitter-receiver designs for highly frequency selective channels in MIMO FBMC systems," *IEEE Trans. Signal Process.*, vol. 60, no. 12, pp. 6519–6532, 2012.

[7] M. Bellanger, "Efficiency of Filter Bank Multicarrier Techniques in Burst Radio Transmission," in *2010 IEEE Global Telecommunications Conference GLOBECOM 2010*, Dec 2010, pp. 1–4.

[8] J. Yli-Kaakinen and M. Renfors, "Optimized burst truncation in fast-convolution filter bank based waveform generation," in *2015 IEEE 16th International Workshop on Signal Processing Advances in Wireless Communications (SPAWC)*, June 2015, pp. 71–75.

[9] M. J. Abdoli, M. Jia, and J. Ma, "Weighted circularly convolved filtering in OFDM/OQAM," in *2013 IEEE 24th Annual International Symposium on Personal, Indoor, and Mobile Radio Communications (PIMRC)*, Sept 2013, pp. 657–661.

[10] D. Waldhauser, L. Baltar, and J. Nossek, "MMSE subcarrier equalization for filter bank based multicarrier systems," in *IEEE 9th Workshop on Signal Processing Advances in Wireless Communications, 2008. SPAWC 2008*. IEEE, 2008, pp. 525–529.

[11] L. Baltar, D. Waldhauser, and J. Nossek, "MMSE subchannel decision feedback equalization for filter bank based multicarrier systems," in *IEEE International Symposium on Circuits and Systems, 2009. ISCAS 2009*. IEEE, 2009, pp. 2802–2805.

[12] A. Ikhlef and J. Louveaux, "An enhanced MMSE per subchannel equalizer for highly frequency selective channels for FBMC/OQAM systems," in *IEEE 10th Workshop on Signal Processing Advances in Wireless Communications, 2009. SPAWC'09*. IEEE, 2009, pp. 186–190.

[13] T. Ihalainen, A. Ikhlef, J. Louveaux, and M. Renfors, "Channel equalization for multi-antenna FBMC/OQAM receivers," *IEEE Trans. Veh. Technol.*, vol. 60, no. 5, pp. 2070–2085, 2011.

[14] F. Horlin, J. Fickers, T. Deleu, and J. Louveaux, "Interference-free SDMA for FBMC-OQAM," *EURASIP Journal on Advances in Signal Processing*, vol. 2013, no. 1, pp. 1–13, 2013. [Online]. Available: http://dx.doi.org/10.1186/1687-6180-2013-46

[15] F. Rottenberg, X. Mestre, and J. Louveaux, "Optimal zero forcing precoder and decoder design for multi-user MIMO FBMC under strong channel selectivity," in *2016 IEEE International Conference on Acoustics, Speech and Signal Processing*, March 2016, pp. 3541–3545.

[16] J. Rodríguez-Piñeiro, M. Lerch, T. Domínguez-Bolaño, J. A. García-Naya, S. Caban, and L. Castedo, "Experimental assessment of 5G-candidate modulation schemes at extreme speeds," in *2016 IEEE Sensor Array and Multichannel Signal Processing Workshop (SAM)*, July 2016, pp. 1–5.

[17] J. Rodríguez-Piñeiro, T. Domínguez-Bolaño, P. Suárez-Casal, J. García-Naya, and L. Castedo, "Affordable Evaluation of 5G Modulation Schemes in High Speed Train Scenarios," in *WSA 2016; 20th International ITG Workshop on Smart Antennas*, March 2016, pp. 1–8.

[18] J. Bazzi, K. Kusume, P. Weitkemper, K. Saito, A. Benjebbour, and Y. Kishiyama, "Performance of multi-carrier waveforms in vehicle-to-vehicle communications," in *Vehicular Networking Conference (VNC), 2015 IEEE*, Dec 2015, pp. 9–16.

[19] E. Kofidis and A. Rontogiannis, "Adaptive BLAST decision-feedback equalizer for MIMO-FBMC/OQAM systems," in *21st Annual IEEE International Symposium on Personal, Indoor and Mobile Radio Communications*, Sept 2010, pp. 841–846.

[20] C. Mavrokefalidis, A. Rontogiannis, E. Kofidis, A. Beikos, and S. Theodoridis, "Efficient adaptive equalization of doubly dispersive channels in MIMO-FBMC/OQAM systems," in *2014 11th International Symposium on Wireless Communications Systems (ISWCS)*, Aug 2014, pp. 308–312.

[21] L. Marijanovi, S. Schwarz, and M. Rupp, "MMSE equalization for FBMC transmission over doubly-selective channels," in *2016 International Symposium on Wireless Communication Systems (ISWCS)*, Sept 2016, pp. 170–174.

[22] L. Zhang, P. Xiao, A. Zafar, A. ul Quddus, and R. Tafazolli, "FBMC System: an insight into doubly dispersive channel impact," *IEEE Trans. Veh. Technol.*, vol. PP, no. 99, pp. 1–1, 2016.

[23] G. Taubock, F. Hlawatsch, D. Eiwen, and H. Rauhut, "Compressive Estimation of Doubly Selective Channels in Multicarrier Systems: Leakage Effects and Sparsity-Enhancing Processing," *IEEE Journal of Selected Topics in Signal Processing*, vol. 4, no. 2, pp. 255–271, April 2010.

[24] M. Fuhrwerk, J. Peissig, and M. Schellmann, "Channel adaptive pulse shaping for OQAM-OFDM systems," in *2014 22nd European Signal Processing Conference (EUSIPCO)*, Sept 2014, pp. 181–185.

[25] A. Şahin, I. Güvenç, and H. Arslan, "A comparative study of FBMC prototype filters in doubly dispersive channels," in *2012 IEEE Globecom Workshops*, Dec 2012, pp. 197–203.

[26] X. Mestre, M. Majoral, and S. Pfletschinger, "An Asymptotic Approach to Parallel Equalization of Filter Bank Based Multicarrier Signals," *IEEE Trans. Signal Process.*, vol. 61, no. 14, pp. 3592–3606, July 2013.

[27] X. Mestre and D. Gregoratti, "Parallelized Structures for MIMO FBMC under Strong Channel Frequency Selectivity," *IEEE Trans. Signal Process.*, vol. PP, no. 99, pp. 1–1, 2015.

[28] D. Petrov, A. Oborina, L. Giupponi, and T. H. Stitz, "Link performance model for filter bank based multicarrier systems," *EURASIP Journal on Advances in Signal Processing*, vol. 2014, no. 1, p. 1, 2014.

[29] D. Petrov, B. Herman, T. Hämäläinen, and S. Melnikz, "On the system level performance of cellular FBMC-based wideband PMR network," in *2015 International Symposium on Wireless Communication Systems (ISWCS)*, Aug 2015, pp. 521–525.
[30] D. Petrov, T. Hämäläinen, and S. Melnik, "Asymptotic Presentation of Intrinsic Interference for FBMC/OQAM Signals in Quasi-Static Channels," in *European Wireless 2016; 22th European Wireless Conference*, May 2016, pp. 1–6.
[31] P. Bello, "Characterization of randomly time-variant linear channels," *IEEE Trans. Commun.*, vol. 11, no. 4, pp. 360–393, 1963.
[32] E. Kofidis, D. Katselis, A. Rontogiannis, and S. Theodoridis, "Preamble-based channel estimation in OFDM/OQAM systems: A review," *Signal Process.*, vol. 93, no. 7, pp. 2038–2054, July 2013. [Online]. Available: http://dx.doi.org/10.1016/j.sigpro.2013.01.013
[33] E. Kofidis, "Channel estimation in filter bank-based multicarrier systems: Challenges and solutions," in *2014 6th International Symposium on Communications, Control and Signal Processing (ISCCSP)*, May 2014, pp. 453–456.
[34] X. Mestre and E. Kofidis, "Pilot-based channel estimation for FBMC/OQAM systems under strong frequency selectivity," in *2016 IEEE International Conference on Acoustics, Speech and Signal Processing (ICASSP)*, March 2016, pp. 3696–3700.
[35] P. Duhamel and M. Vetterli, "Fast Fourier transforms: a tutorial review and a state of the art," *Signal Proces.*, vol. 19, no. 4, pp. 259–299, 1990.
[36] P. Siohan, C. Siclet, and N. Lacaille, "Analysis and design of OFDM/OQAM systems based on filterbank theory," *IEEE Trans. Signal Process.*, vol. 50, no. 5, pp. 1170–1183, 2002.
[37] "Universal Mobile Telecommunications System (UMTS); Deployment aspects (3GPP TR 25.943 version 13.0.0 Release 13)," ETSI, Tech. Rep., 2016.
[38] M. G. Bellanger, "Specification and design of a prototype filter for filter bank based multicarrier transmission," in *IEEE International Conference on Acoustics, Speech, and Signal Processing*, vol. 4. IEEE, 2001, pp. 2417–2420.
[39] M. Fuhrwerk, J. Peissig, and M. Schellmann, "Performance comparison of CP-OFDM and OQAM-OFDM systems based on LTE parameters," in *2014 IEEE 10th International Conference on Wireless and Mobile Computing, Networking and Communications (WiMob)*, Oct 2014, pp. 604–610.
[40] M. Fuhrwerk, S. Moghaddamnia, and J. Peissig, "Scattered Pilot-Based Channel Estimation for Channel Adaptive FBMC-OQAM Systems," *IEEE Trans. Wireless Commun.*, vol. 16, no. 3, pp. 1687–1702, March 2017.
[41] F. Rottenberg, X. Mestre, F. Horlin, and J. Louveaux, "Single-Tap Precoders and Decoders for Multiuser MIMO FBMC-OQAM Under Strong Channel Frequency Selectivity," *IEEE Trans. Signal Process.*, vol. 65, no. 3, pp. 587–600, Feb 2017.

Xavier Mestre (S'96M'03SM'09) received the MS and PhD in Electrical Engineering from the Technical University of Catalonia (UPC) in 1997 and 2002 respectively and the Licenciate Degree in Mathematics in 2011. During the pursuit of his PhD, he was recipient of a 1998-2001 PhD scholarship (granted by the Catalan Government) and was awarded the 2002 Rosina Ribalta second prize for the best doctoral thesis project within areas of Information Technologies and Communications by the Epson Iberica foundation. From January 1998 to December 2002, he was with UPC's Communications Signal Processing Group, where he worked as a Research Assistant. In January 2003 he joined the Telecommunications Technological Center of Catalonia (CTTC), where he currently holds a position as a Senior Research Associate in the area of Radio Communications. During this time, he has actively participated in multiple European projects and several contracts with the local industry. Currently, he is head of the Advanced Signal and Information Processing Department. He has been associate editor of IEEE Transactions on Signal Processing, 2007-2011, 2015-present and an elected member of the IEEE Sensor Array and Multichannel Signal Processing Technical Committee.

Dmitry Petrov graduated from the Physical faculty of M.V. Lomonosov Moscow state university in 2007. He received his Ph.D. degree (2010) from the same university. In 2009-2011, Dr. Petrov was an invited expert in several projects, where he developed mathematical models for telecommunication and financial sectors. Dmitry Petrov got his second Ph.D. degree (2012) and the title of adjunct professor in wireless networking technologies (2016) from the University of Jyvskyl, Finland. In 2011, he joined Magister Solutions Ltd. as a senior researcher. He contributed to several prize-winning European projects and also worked in industrial R&D projects. In 2017 he started his work at Nokia. The main areas of scientific interests for Dr. Petrov are multi-carrier systems with advanced wave-forms, signal processing, computer simulations of wireless networks, and innovation in technology. He also continues academic work in cooperation with several universities. He is a co-author of more than 30 academic publications in peer-reviewed journals and international conferences.

François Rottenberg (S'15) received the M.Sc. in electrical engineering from the Université catholique de Louvain (UCL), Louvain-la-Neuve, in 2014. Since September 2014, he is a Ph.D. student working part time at ICTEAM - Université catholique de Louvain and at OPERA - Université libre de Bruxelles. From September 2014 to February 2015, he participated to the ICT-EMPhAtiC European project on Enhanced Multicarrier Techniques for Professional Ad-Hoc and Cell-Based Communications. In 2015, he was a visitor at CTTC, Spain. His current research interests are in signal processing for communications including MIMO and filter bank-based multicarrier systems.

François Horlin (S'01M'02) received the electrical engineering degree and the Ph.D. degree from the Université catholique de Louvain (UCL), Louvain-la-Neuve, Belgium, in 1998 and 2002 respectively. During his studies, he specialised in the field of digital signal processing for communications. In 2002, he joined the Inter-university Micro-Electronics Center (IMEC), Leuven, Belgium. He led the project aiming at developing a fourth-generation wireless communication system in collaboration with Samsung Korea. In 2007, Franois Horlin became associate professor at the Université libre de Bruxelles (ULB), Brussels, Belgium. Since 2014, he is full professor. He is currently giving three lectures in the field of digital telecommunications and is advisor of 6 Ph.D. students (plus 13 already defended Ph.D. theses). He is author of a book, author of a book chapter, co-author of two patents, author or co-author of more than 180 publications in well-recognised journals and conferences. He currently chairs the IEEE signal processing chapter of the Benelux.

This article has been accepted for publication in a future issue of this journal, but has not been fully edited. Content may change prior to final publication. Citation information: DOI 10.1109/TSP.2017.2711534, IEEE Transactions on Signal Processing

Jérôme Louveaux (S'98-M'02) received the electrical engineering degree and the Ph. D. degree from the Universit catholique de Louvain (UCL), Louvain-la-Neuve, Belgium in 1996 and 2000 respectively. From 2000 to 2001, he was a visiting scholar in the Electrical Engineering department at Stanford University, CA. From 2004 to 2005, he was a postdoctoral researcher at the Delft University of technology, Netherlands. Since 2006, he has been a Professor in the ICTEAM institute at UCL. His research interests are in signal processing for digital communications, and in particular: multicarrier modulations, xDSL systems, resource allocation, synchronization and estimation. Prof. Louveaux was a co-recipient of the "Prix biennal Siemens 2000" for a contribution on filter-bank based multi-carrier transmission and co-recipient of the the "Prix Scientifique Alcatel 2005" for a contribution in the field of powerline communications.